Report

Cell Reports

The Role of Ceramide Synthases in the Pathogenicity of *Cryptococcus neoformans*

Graphical Abstract

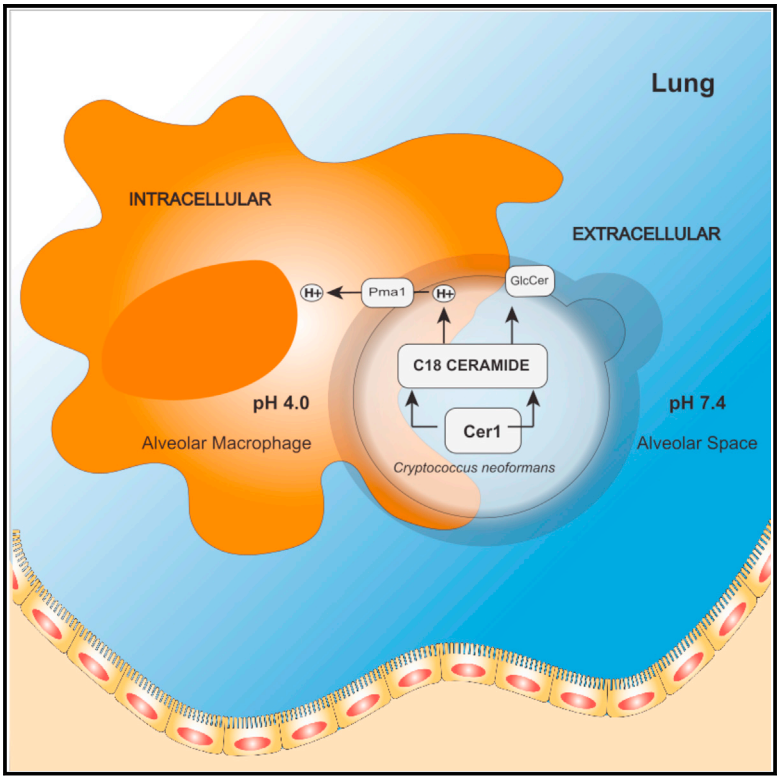

Highlights

- Characterization of *Cryptococcus neoformans* (*C. neoformans*) ceramide synthases
- A virulence role for ceramides in *C. neoformans* infection
- Ceramide pathway affects Pma1 activity
- *Cer1* primarily produces ceramides with chain lengths of 18 carbons

Authors

Mansa A. Munshi, Justin M. Gardin, Ashutosh Singh, ..., Tejas Bouklas, Bettina C. Fries, Maurizio Del Poeta

Correspondence

maurizio.delpoeta@stonybrook.edu

In Brief

Cryptococcus neoformans (*C. neoformans*) is a fungal pathogen that causes about 220,000 deaths annually in immunocompromised individuals. Munshi et al. explore fungal lipid metabolism in the context of *C. neoformans* pathogenicity.

Munshi et al., 2018, Cell Reports *22*, 1392–1400
February 6, 2018
https://doi.org/10.1016/j.celrep.2018.01.035

CellPress

OPEN ACCESS
CellPress

Cell Reports
Report

The Role of Ceramide Synthases in the Pathogenicity of *Cryptococcus neoformans*

Mansa A. Munshi,[1] Justin M. Gardin,[2] Ashutosh Singh,[3] Chiara Luberto,[4] Robert Rieger,[5] Tejas Bouklas,[6] Bettina C. Fries,[1,7] and Maurizio Del Poeta[1,7,8,9,*]

[1]Department of Molecular Genetics and Microbiology, Stony Brook University, Stony Brook, NY 11794, USA
[2]The Jackson Laboratory, Bar Harbor, ME 04609, USA
[3]Department of Biochemistry, University of Lucknow, Lucknow, Uttar Pradesh 226007, India
[4]Department of Physiology and Biophysics, Stony Brook University, Stony Brook, NY 11794, USA
[5]Proteomics Center, Stony Brook University, Stony Brook, NY 11794, USA
[6]Department of Biomedical Sciences, School of Health Professions and Nursing, Long Island University, Brookville, NY 11548, USA
[7]Division of Infectious Diseases, School of Medicine, Stony Brook University, Stony Brook, NY 11794, USA
[8]Veterans Administration Medical Center, Northport, NY 11768, USA
[9]Lead Contact
*Correspondence: maurizio.delpoeta@stonybrook.edu
https://doi.org/10.1016/j.celrep.2018.01.035

SUMMARY

***Cryptococcus neoformans* (*C. neoformans*) is estimated to cause about 220,000 new cases every year in patients with AIDS, despite advances in antifungal treatments. *C. neoformans* possesses a remarkable ability to disseminate through an immunocompromised host, making treatment difficult. Here, we examine the mechanism of survival of *C. neoformans* under varying host conditions and find a role for ceramide synthase in *C. neoformans* virulence. This study also provides a detailed lipidomics resource for the fungal lipid research community in addition to discovering a potential target for antifungal therapy.**

INTRODUCTION

Cryptococcus neoformans (*C. neoformans*) is a pathogenic fungus that presents a leading cause of fungal meningoencephalitis worldwide. Recent reports reveal an annual 278,000 cases of cryptococcal antigenemia, with cryptococcal meningitis being the cause of 15% of AIDS-related deaths (Rajasingham et al., 2017). Naturally occurring cases of cryptococcosis begin by inhalation of fungal spores. Once in the lung, the outcome depends largely on the immune system of the individual. In a situation of suppressed immunity, infection may lead to pneumonia and cryptococcal meningitis. In cases of immunocompetence, these cells are either cleared or may establish a latent infection that will later disseminate upon future immunosuppression.

Once *C. neoformans* enters the lung, the cells are typically engulfed by an alveolar macrophage in which they can survive and replicate. Similarly, *C. neoformans* can survive and replicate well in extracellular spaces, such as alveoli, blood, and other tissues. Once engulfed, *C. neoformans* can move between the phagolysosome and extracellular space without causing harm to the macrophage (Alvarez and Casadevall, 2006; Feldmesser et al., 2000). The intracellular and extracellular environment in the host is distinguished by a prominent difference in pH. Within the phagolysosome, the environment pH is highly acidic, whereas the extracellular environment is typically neutral or slightly alkaline. Adaptation to these starkly contrasting environments is critical for *C. neoformans* pathogenicity. There is little information regarding how *C. neoformans* regulates its survival in these two host environments. Previous studies have shown sugar-complexed sphingolipids to be essential for the survival of *C. neoformans* when grown in media mimicking host acidic or alkaline conditions. Specifically, inositol- or mannose-containing sphingolipids are noted as important for the survival and replication of *C. neoformans* in conditions similar to the phagolysosome (Luberto et al., 2001). Conversely, glucose-containing sphingolipids have been indicated to be important for survival in conditions mimicking the extracellular environment (Rittershaus et al., 2006). Among sphingolipids, ceramides constitute the simplest class and the basic backbone that precedes other more complex sphingolipids (Aguilera-Romero et al., 2014). Acyl coenzyme A (CoA)-dependent ceramide synthases catalyze the formation of ceramide from a fatty acyl CoA and sphingoid base. Cryptococcal sphingolipids regulate signaling events that lead to the production of virulence factors (Singh and Del Poeta, 2011). Studies in *C. albicans* (Cheon et al., 2012), *S. cerevisiae* (Kageyama-Yahara and Riezman, 2006), *A. nidulans* (Li et al., 2006), and *P. pastoris* (Ternes et al., 2011) show the presence of two distinct ceramide synthase enzymes.

Although a handful of studies reveal different characteristic functions of ceramide synthases in each eukaryotic species, there is still a lack of concrete evidence for the specific roles of ceramide synthases in the context of sphingolipid biosynthesis of fungi. In this study, we identify and characterize the ceramide synthases of *C. neoformans*, thereby elucidating several steps in the sphingolipid biosynthetic pathway. We show that the major ceramide synthase of this pathogen is a critical player in its pathogenicity, as well as the hub of numerous cellular functions. We further highlight how a single gene has the capacity to control the dissemination of *C. neoformans*, therefore suggesting a therapeutic target.

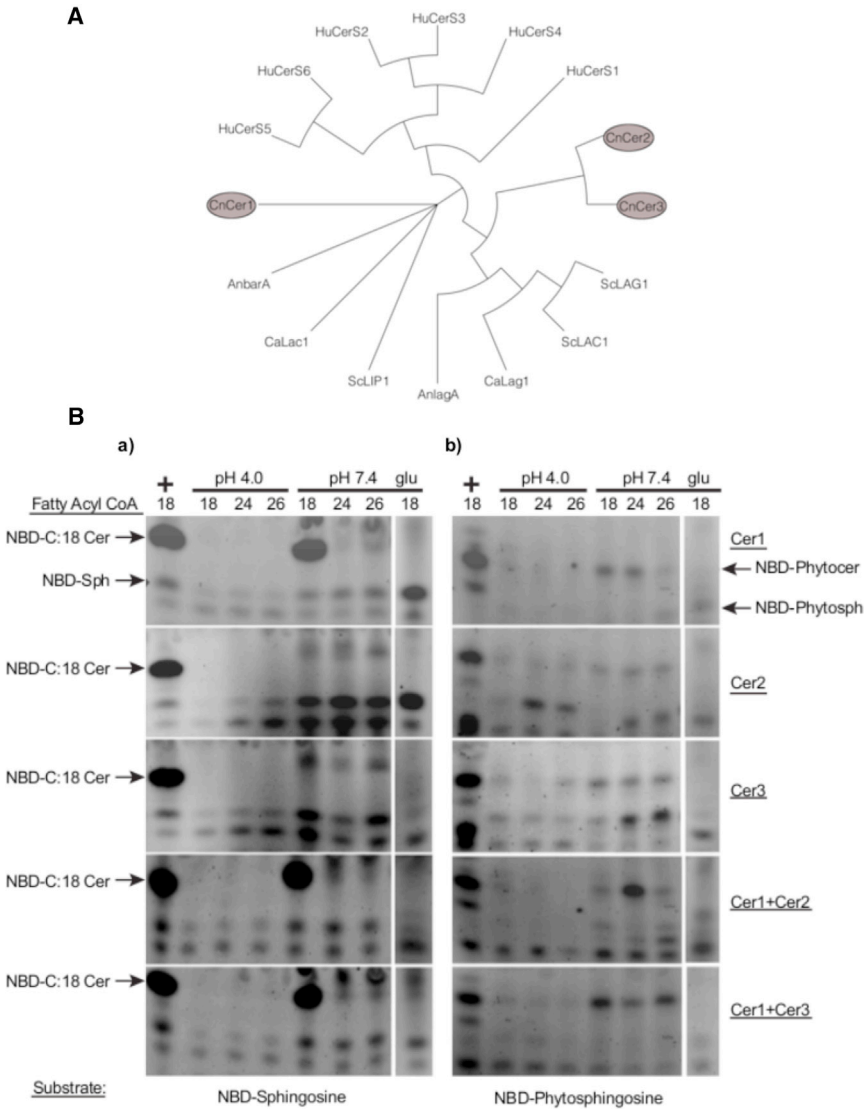

Figure 1. Isolation and Characterization of *C. neoformans* Ceramide Synthases

(A) Phylogenetic analysis of eukaryotic ceramide synthases. *C. neoformans* has three ceramide synthases. The entire phylogenetic tree can be roughly divided into three major groups: human cerS genes, the second group containing orthologs of *Cn*Cer1, and the third group consisting of *S. cerevisiae* Lac1 and Lag1, *An*LagA, *Ca*Lac1, and *Cn*Cer2 and *Cn*Cer3. *ScLip1* is distinct from all of these genes.

(B) Biochemical analysis of *C. neoformans* ceramide synthases. Thin-layer chromatography showing substrate specificity studies of *C. neoformans* ceramide synthases. (a) Ceramide synthase assays using NBD-sphingosine as a substrate. Lane 1 (left) is positive control using mammalian *Cer1* microsomes. Negative control of each strain grown in 2% glucose (right) (see also Figure S3). (b) Ceramide synthase assays using NBD-phytosphingosine as a substrate. Lane 1 (left) is positive control using mammalian *Cer1* microsomes. Negative control of each strain grown in 2% glucose (right). Each horizontal panel represents a specific strain.

RESULTS

Three Genes in *C. neoformans* Encode Specific Acyl-CoA-Dependent Ceramide Synthases

On the basis of evidence of ceramide synthases in other fungi, we performed a bioinformatic search for putative ceramide synthases present in *C. neoformans* serotype A H99 (WT). Our analysis revealed the presence of three putative ceramide synthases in *C. neoformans*. The genes CNAG_06717, CNAG_02086, and CNAG_02087 had significant homology to other ceramide synthase genes from *A. nidulans*, *C. albicans*, *S. cerevisiae*, and *H. sapiens* (Figure 1A). They are referred to in this study as *Cer1*, *Cer2*, and *Cer3*, respectively. A phylogenetic analysis showed that *Cer2* and *Cer3* have high similarity to each other, as well as to ceramide synthases of *S. cerevisiae* (*Sc*Lac1 and *Sc*Lag1) and *A. nidulans* (*An*LagA). The *Cer1* amino acid sequence is greatly diverged from *Cer2* and *Cer3* and has partial similarity to ceramide synthases of *C. albicans* (*Ca*Lag1) and *A. nidulans* (*An*BarA). Reports on these genes show a distinct specificity for synthesis of ceramides used for glucosylceramide (GlcCer) synthesis (Figure 1A) (Li et al., 2006; Rittenour et al., 2011; Cheon et al., 2012). An alignment of the amino acid sequences of these genes revealed conservation of residues that are reportedly important for enzymatic activity (Figure S1D) (Kageyama-Yahara and Riezman, 2006).

Ceramide Synthase *Cer1* Activity *In Vitro* Shows Preference for C18 Fatty Acyl CoA

To characterize the activity of each enzyme, we generated strains overexpressing each *C. neoformans* ceramide synthase in *S. cerevisiae* using either a 6xHis or 3xHA tag fused protein. These plasmids were transformed in combination into the *S. cerevisiae* system to generate strains overexpressing both *Cer1-Cer2* or *Cer1-Cer3*. After induction, the proteins were purified by extraction of microsomes (Ternes et al., 2011). As a negative control, these strains were grown without induction (2% glucose) and were used to control for any *S. cerevisiae* enzyme activity (Figures S3A and S3B).

To characterize the properties of the putative ceramide synthases, an *in vitro* assay for fungal ceramide synthase was developed (see Experimental Procedures). Using a fluorescent-labeled substrate and fatty acyl CoA, we looked for the formation of NBD-ceramide using microsomal *C. neoformans* ceramide synthase enzyme by thin-layer chromatography. We observed that the activity of *Cer1* is dependent on pH (Figure 1B) and temperature (Figure S3C). The activity of *Cer1* was optimal at pH 7.0 and 35°C.

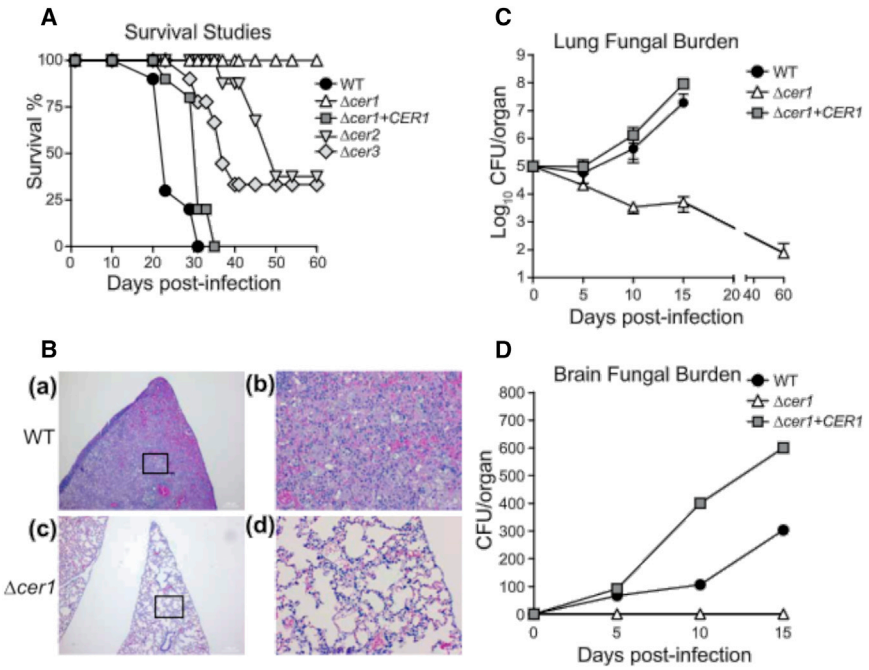

Figure 2. Ceramide Synthases Are Important for Virulence of *C. neoformans*

(A) Survival studies of CBA/JCrHsd mice infected intranasally with WT, *Δcer1*, *Δcer1* + *CER1*, *Δcer2*, and *Δcer3*. n = 10 mice per group.

(B) Histology of lung tissue for WT (at time of death) and for *Δcer1* (day 60). Lung sections were stained with H&E. (a and b) Lung of mice infected with WT. (c and d) Lung of mice infected with *Δcer1*. Bars, 1,000 μm (a and c), 20 μm (b and d).

(C) Lung tissue burden analysis of WT, *Δcer1*, and *Δcer1+CER1*. Data are expressed as mean ± SEM.

(D) Brain fungal burden analysis of WT, *Δcer1*, and *Δcer1+CER1*. n = 3 mice at each time point.

See also Figure S2.

To systematically investigate each enzyme's specificities, we used combinations of fatty acyl CoAs, with either sphingosine or phytosphingosine at pH 4.0 or 7.0. *Cer1* showed a clear preference for C18 fatty acyl CoA and sphingosine as a substrate (Figure 1Ba). When phytosphingosine was used a substrate, we observed production of C18 and C24 phytoceramide in slightly lower amounts (Figure 1Bb). When *Cer1* and *Cer2* were co-expressed, C24 phytoceramide was the major product. However, when *Cer1* and *Cer3* were co-expressed, the enzyme activity shifted to C18 and C26 fatty acyl CoA products (Figure 1Bb). These results suggest that the production of ceramide isoforms is regulated by the stoichiometry of the three ceramide synthase proteins of *C. neoformans* in the presence of different substrate chain lengths. Uninduced cells (2% glucose) showed little to no enzyme activity under these conditions (Figure 1B).

Ceramide Synthases Are Important for the Virulence of *C. neoformans*

To determine the effect of each ceramide synthase on the virulence of *C. neoformans*, we created ceramide synthase deletion strains in the WT *C. neoformans* background (Figures S1A–S1C). Each cell line, containing a deletion cassette or a reintroduced ceramide synthase gene, was tested on CBA/JCrHsd immunocompetent mice. Mice were infected with a normally lethal dose of fungal cells (7×10^5 cells) intranasally to establish cryptococcosis and were monitored for survival. We observed that the average survival of mice infected with WT *C. neoformans* was 25 ± 6 days, while all mice infected with *Δcer1* survived (60 days of observation) (Figure 2A). The average survival of mice infected with the reconstructed gene strain *Δcer1+CER1* experienced mortality similar to the WT control, with an average survival of 26 ± 7 days (Figure 2A). Mice infected with *Δcer2* and *Δcer3* showed a survival pattern distinct from WT (Figure 2A), with each deletion causing ~70% mortality.

Tissue burden was assessed throughout the course of the experiment by removal of lungs and brain at days 0, 5, 10, and 15 post-infection. The number of *Δcer1* cells in the lung decreased starting at day 5 and was reduced to ~3,500 colony-forming units (CFU)/lung at day 15, showing a decrease in lung CFU of 250-fold. At day 60, we recovered fungal cells in the lung (~500 CFU) but in only two of ten mice, suggesting that most mice cleared the infection (Figure 2C). In contrast to WT *C. neoformans* infection, *Δcer1*-infected mice showed no obvious signs of discomfort throughout the course of the experiment and were visually indistinguishable from uninfected mice. The *Δcer1* cells were never observed to progress to the brain of infected mice (Figures 2D and S3A). In contrast, a significant number of cells were found in the lungs and brain of mice infected with WT and *Δcer1+CER1* strains (Figures 3C and 3D). In both these control experiments, the number of cells in the brain increased over time, demonstrating a normal dissemination and subsequent onset of cryptococcosis. These observations were also confirmed by histopathology of the brain and lung, in which we observed no damage to the lungs and brains of mice infected with *Δcer1* (Figure 2B). Mice infected with WT and *Δcer1+CER1* showed significant lung and brain tissue damage (Figures 2B and S3).

To understand the inflammatory response to *C. neoformans* infection in the lungs, histopathology was performed at days 1, 3, 5, and 60 (only *Δcer1* mice survived to day 60). Lungs of *Δcer1*-infected mice showed a high degree of immune cell infiltrate to the lung and alveolar spaces. As the experiment progressed, we observed progressive clearing of the immune cell infiltrate (Figures 2B and S3B). Cells of *Δcer1* could be observed in several areas of the lung until day 5. These cells appeared to have difficulty completing replication and had a pseudohyphal morphology. Lungs infected with WT showed a persistently high level of immune cell infiltrate throughout the time course, enlarged *C. neoformans* capsules, and fungal pneumonia, which was not observed for *Δcer1* (Figure S2B). The total burden of WT *C. neoformans* cells increased throughout the time course (Figure 2).

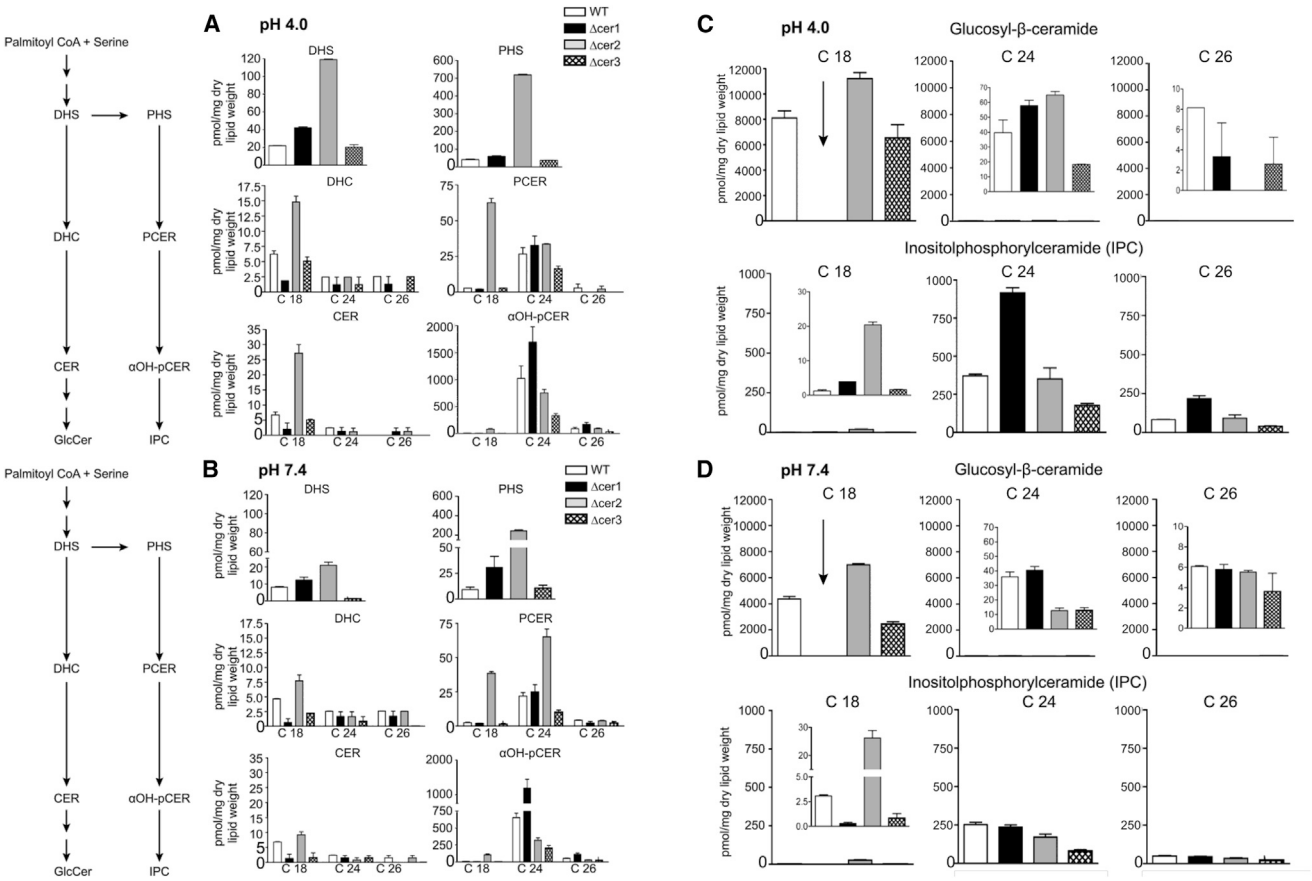

Figure 3. Sphingolipid Biosynthetic Pathway and Ceramide Species Abundance of *C. neoformans* Ceramide Synthase Mutants and WT in Distinct Host Conditions *In Vitro* Using MS Analysis

(A) Changes in specific lipid classes at pH 4.0.

(B) Changes in specific lipid classes at pH 7.4.

(C and D) Abundance of complex sphingolipid species in WT and ceramide synthase mutants at pH 4.0 (C) and 7.4 (D). All the lipids are normalized to dry lipid weight.

Data are expressed as mean ± SEM. αOH-PCER, α-hydroxy-phytoceramide; CER, ceramide; DHC, dihydroceramide; DHS, dihydrosphingosine; GlcCer, glucosylceramide; IPC, inositolphosphoryl ceramide; PCER, phytoceramide; PHS, phytosphingosine. See also Figure S4 and Tables S2 and S3.

Identification of Lipid Changes on Ceramide Synthase Deletion

The sphingolipid pathway in *C. neoformans* can be separated into two major branches: substrates that lead to the generation of glucose-containing sphingolipids such as GlcCer and those that lead to inositol-containing sphingolipids such as inositol phosphorylceramide (IPC). To assess the specific roles of each gene in lipid metabolism, we analyzed each knockout strain with lipidomic-focused mass spectrometry. The analysis was performed on cells grown in *in vitro* conditions (5% CO_2, 37°C, DMEM) mimicking host-like growth conditions.

Because fungal cells produce a diverse array of ceramide species, we developed mass spectrometry detection protocols for an array of the most abundant ceramide lipids. When exposed to an acidic environment, WT *C. neoformans* showed accumulation of dihydrosphingosine as well as higher total biomass of GlcCer species (Figure 3). We also observed higher abundance of phytosphingosine and certain long-chain α-OH phytoceramides (C24, C26). This increase was propagated downstream in the pathway by increased levels of 42:0:4, 42:0:5, and 44:0:4 chain length IPCs (Figures 3 and S4). In contrast, at alkaline pH, sphingosine-1-phosphate, dihydrosphingosine-1-phosphate, and phytosphingosine-1-phosphate were twice as abundant as those in acidic pH (Figure S4). Therefore, the data show not only that *C. neoformans* changes the metabolism of several lipid species when it is exposed to different host conditions but, more important, that this change depends on specific ceramide isoforms to generate sufficient amounts of the resulting complex sphingolipids. The lipid profile of *Δcer1* was significantly perturbed from WT compared with the milder phenotypes of *Δcer2* and *Δcer3*. We observed that *Cer1* was the major ceramide synthase responsible for using C18 fatty acyl CoA to generate C18 ceramides (Figures 1B and 3). As C18 ceramides are required to synthesize aOH-C19:2/C18 GlcCer, the most abundant GlcCer in either condition, the strain *Δcer1* is lacking the vast majority of its normal glucose-containing complex

sphingolipids (Figure 3C). C24 and C26 lipids were not significantly depleted in the *Δcer1* strain but also represented a tiny fraction of total GlcCer abundance in the WT strain (Figure 3C). This observation agrees with the *in vitro* findings of chain-length specificity for *Cer1* (Figure 1B). In the *Δcer1* strain, depletion of IPCs generated from non-hydroxylated and α-hydroxylated C18 phytoceramides contrasts with the accumulation of long-chain IPCs. Notably, *Δcer1* and *Δcer3* showed a significant depletion of C26 phytoceramides in acidic conditions (Figure 3A).

These data indicate that upon loss of *Cer1*, *Cer2* and *Cer3* can partially compensate for production of certain sphingolipid isoforms but are insufficient for production of the major C18 ceramide isoforms. Broadly speaking, of the lipid isoforms showing significant change, these changes were most pronounced under acidic conditions (Figures 3 and S5). The levels of the major IPC, IPC 42:0:4, remained relatively unchanged in the deletion strains. *Δcer2* showed little to no depletion of lipids but a marked increase in dihydrosphingosine, C18 dihydroceramide, and total short-chain GlcCers. Additionally, *Δcer2* showed a clear abundance of most C18 lipids in the IPC pathway: phytosphingosine, phytoceramides, αOH phytoceramides, and C36 IPCs all were significantly more abundant compared with WT. Meanwhile, *Δcer3* showed a decrease in lipids along the GlcCer branch of the pathway as well as a decrease in C24 and C26 lipids in the IPC pathway under alkaline conditions. Together, these data suggest that *Cer1* is critical for the biosynthesis of C18 ceramides, where *Δcer2* and *Δcer3* show more subtle lipid phenotypes and appear to fine-tune the abundance of less common lipids (Figure S4; Data S1).

Effect of Ceramide Synthase on the *In Vitro* Growth of *C. neoformans*

To evaluate the effect of gene deletion in *in vitro* cell culture growth, we performed growth assays of *C. neoformans* WT, *Δcer1*, and *Δcer1+CER1* strains. Growth was analyzed in conditions mimicking host intracellular and extracellular conditions, using DMEM at neutral/alkaline or acidic conditions at 37°C and 5% CO_2. As shown in Figures 4A and 4B, *Δcer1* cells showed a distinct lack of growth at both conditions mimicking host environments. *Δcer1* viability began to decrease at 24 hr in acidic as well as alkaline conditions. Loss of viability was not observed at 30°C and atmospheric level of CO_2 (Figure 4C). These results indicate the deletion of *Δcer1* is important for the survival and proliferation of *C. neoformans* in host intracellular and extracellular conditions.

To determine the effect of cell wall stress on the deletion strains, a spot assay was performed by exposing WT, *Δcer1*, and *Δcer1+CER1* to 0.03% SDS. We observed that *Δcer1* was more sensitive to cell wall stress compared with WT and *Δcer1+CER1* (Figure 4D). We tested the resilience of these strains to oxidative stress by exposing dilutions of these cells to hydrogen peroxide at pH 4 and 7.4 (Figure 4D). *Δcer1* was hypersensitive to oxidative stress at both pH values. The hypersensitivity of *Δcer1* to low pH and other stresses are significant considering that the spot assay was done using rich medium (YPD) because it could not be performed in minimum medium for the growing defect phenotype of the mutant.

Phenotype Analysis of Ceramide Synthase Mutant Strains

To assess the physiological effects of the deletion of ceramide synthase genes, we analyzed the phenotypes of these cells under several conditions with a focus on alteration of virulence factors. The deletion of *Cer1*, but not *Cer2* or *Cer3*, generated defects in cell morphology. Capsule visualization by India ink staining revealed that cells of *Δcer1* had cell division defects leading to the development of elongated cells with a smaller capsule (Figure S5B). When *Δcer1* was grown in rich medium (YPD), the cells showed normal morphology, with a few cells showing multiple enlarged buds that remained attached. However, upon transfer to host-like growth conditions (5% CO_2, 37°C, DMEM), *Δcer1* cells showed gross morphological defects and inability to complete cytokinesis. A lifespan study of these cells showed that the average replicative lifespan (RLS) of *Δcer1* was only 6.5 generations, whereas those of WT and *Δcer1+CER1* were 27 and 30 generations respectively (Figure S5A). For *Δcer1*, after 6.5 ± 2 generations, the cells formed elongated pseudohyphal-like structures in which new buds were impossible to separate from the mother cell. Despite the inability to separate, the cells continued to elongate for several hours.

We performed transmission electron microscopy to further observe these changes in cellular structure. *Δcer1* cells showed detachment of the cell wall from the plasma membrane in many cells. The elongated "hyphal-like" structures observed in histological and India ink staining were found to be daughter cells that were unable to complete cytokinesis. Interestingly, we also observed that the cell wall structure of *Δcer1* looked very different from that of WT. Although the WT cells showed well-defined, distinct layers resulting in a compact cell wall, the cell wall of *Δcer1* appeared less compact, with no clear separation between cell wall layers (Figure 4E). The fibrillar structures forming the polysaccharide capsule were smaller and less distinct than that of WT (Figure 4E). We hypothesize that the layers of the cell wall of *Δcer1* are inhibitory to cytokinesis and cell separation under two conditions: when the cells are exposed to host-like conditions and when cells are grown in the absence of rich, ceramide lipid-containing media. To confirm the role of ceramides in the formation of such a drastic cellular defect, the cells of *Δcer1* were supplemented with a cocktail of natural ceramides (Matreya). Upon supplementation, we observed that many of the previously observed cellular defects were recovered (Figure 4E). This cocktail predominantly contains a mixture of C18 and C24 hydroxylated and non-hydroxylated ceramides. Together these observations suggest that ceramides synthesized by *Cer1* are critical for proper cytokinesis in stressful host conditions, in which increased cell wall thickness introduces a hindrance for proper daughter cell budding.

C18 Ceramides Generated by *Cer1* Are Important for Acidic Tolerance of *C. neoformans*

We checked the efficiency of the plasma membrane proton pump, Pma1, upon deletion of a ceramide synthase in *C. neoformans*. Pma1 is a crucial mediator of *C. neoformans* virulence, as the proton pump regulates *C. neoformans* cytosolic pH. This is a particularly important function for *C. neoformans* growth inside acidic macrophage lysosomes. A colorimetric pH indicating dye was

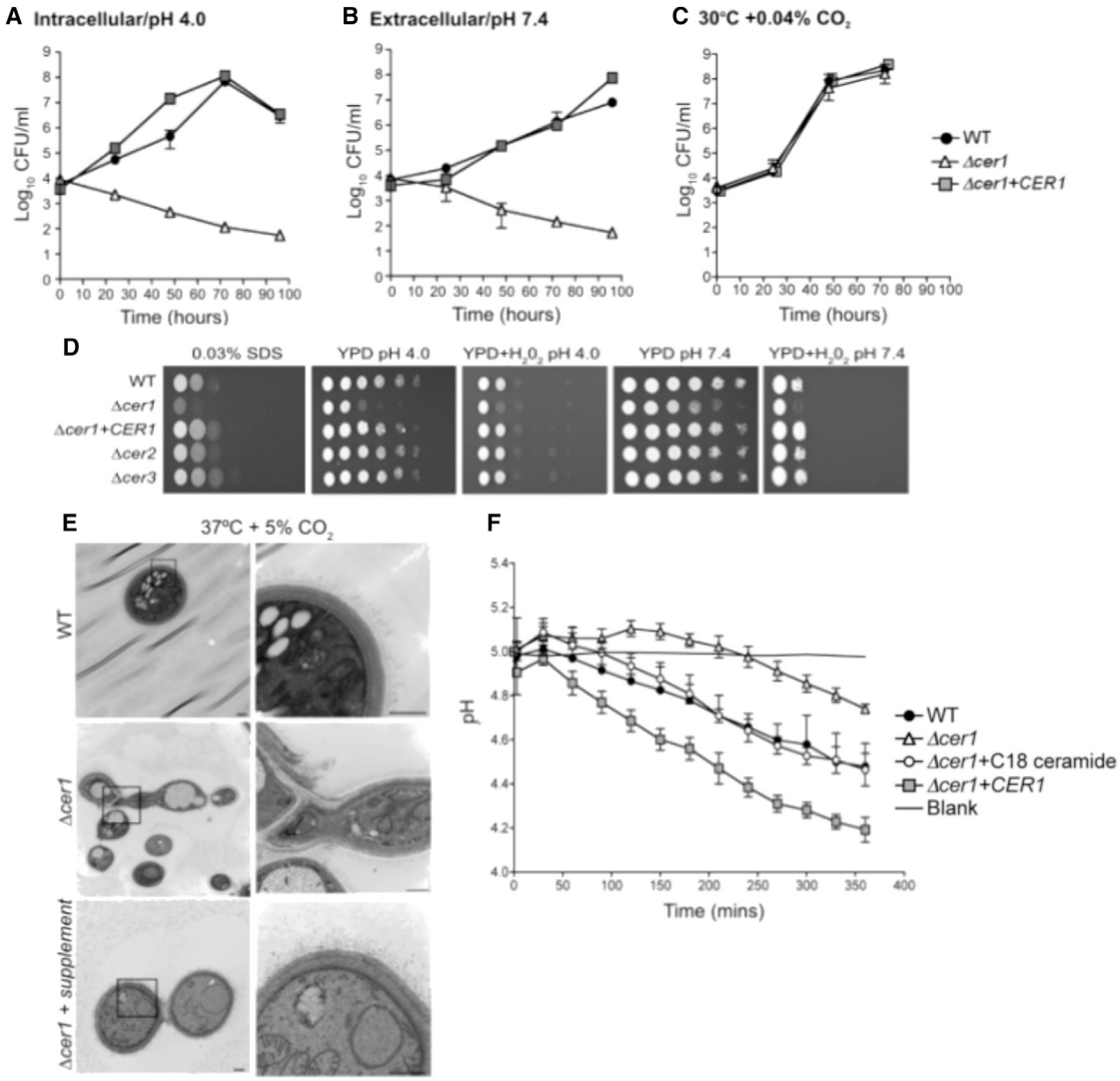

Figure 4. Phenotypic Analysis of Ceramide Synthase Mutants

(A) *In vitro* growth of WT, *Δcer1*, and *Δcer1+CER1* at 37°C, 5% CO_2, pH 4.0 (intracellular).

(B) *In vitro* growth of WT, *Δcer1*, and *Δcer1+CER1* at 37°C, 5% CO_2, pH 7.4 (extracellular).

(C) *In vitro* growth of WT and Δcer1 in YPD, 30°C, 0.04% CO_2.

(D) Serial dilutions of WT, *Δcer1*, *Δcer1 +CER1*, *Δcer2*, and *Δcer3* on solid YPD media supplemented with SDS or H_2O_2.

(E) Transmission electron microscopy of WT, *Δcer1*, and *Δcer1* supplemented with ceramide mixture (Matreya). Bar, 500 nm.

(F) Pma1 proton pump activity of WT, *Δcer1*, *Δcer1+CER1*, and *Δcer1* + C18 ceramide (Avanti Polar Lipids) measured by glucose-dependent medium acidification. Data are expressed as mean ± SEM.

For (A)–(C), data are expressed as mean ± SEM.

used to measure glucose-dependent proton efflux over a time course (Soteropoulos et al., 2000). Our results showed that *Δcer1* cells acidify medium at a much slower rate than WT and *Δcer1+CER1* strains (Figure 4F). We observed an increase in Pma1 efficiency in *Δcer1* cells upon supplementation with C18 ceramide (Figure 4F). To further confirm to the role of ceramides in the observed phenotypes, we tested Pma1 activity of *Δgcs1* strain, as well as the *Δgcs1* strain treated with an IPC1 inhibitory drug, aureobasidin A (AbA). We observed that *Δgcs1* had high Pma1 activity, which was reduced upon treatment with AbA (Figure 5A). Interestingly, supplementation with C18 ceramides, but not phytoceramides, increased Pma1 activity of AbA-treated *Δgcs1* cells (Figure 5A). To ensure that the Pma1 activity data were not attributable to higher or lower rates of cell death, we measured cell viability at the end of each experiment and found no difference between strains (data not shown). To further clarify the role of intermediate ceramides, we used a genetically downregulated IPC1 strain (*GAL7::IPC1*) that has been reported to show reduced growth in acidic conditions. The growth defect of this strain was compensated by supplementation C18 ceramide and to a smaller extent by C6 phytoceramide (Figure 5B). These data indicate that the intermediate ceramide isoforms, not the terminal

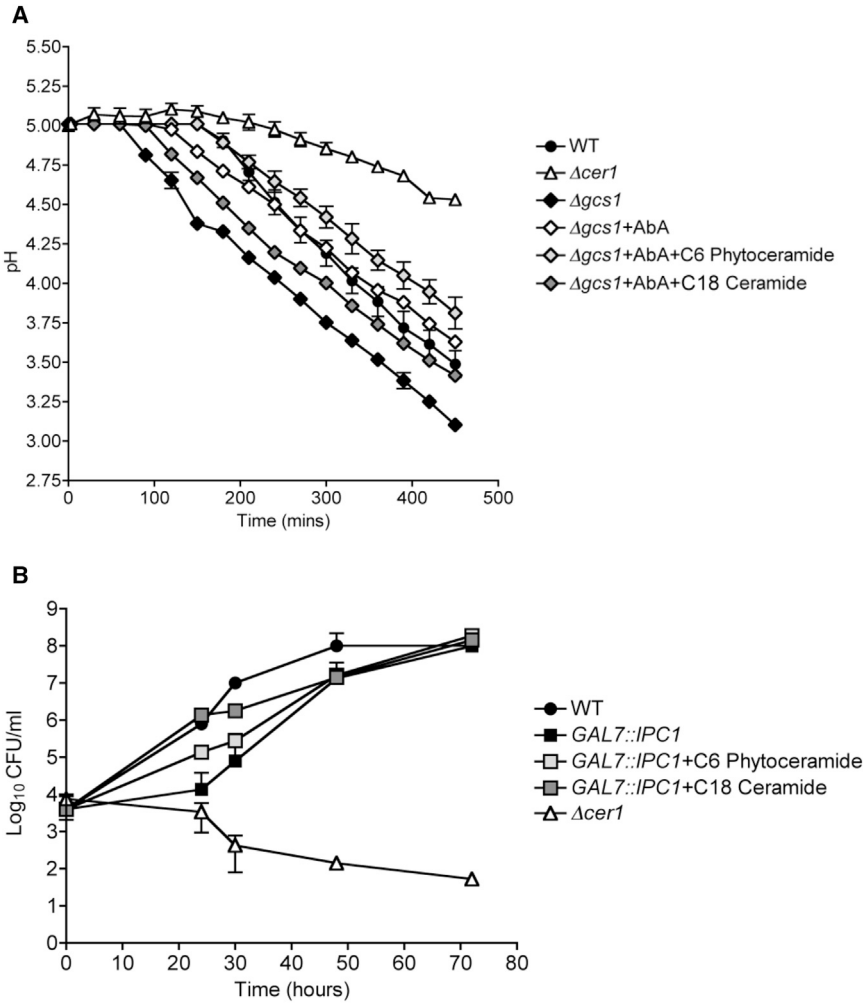

Figure 5. Effect of Ceramide on Pma1 Activity and on Cell Growth

(A) Pma1 proton pump activity of WT, *Δcer1*, *Δgcs1*, *Δgcs1*+AbA, *Δgcs1*+AbA+C6 phytoceramide, and *Δgcs1*+AbA+C18 ceramide measured by glucose-dependent medium acidification. Data are expressed as mean ± SEM.

(B) *In vitro* growth of WT, *GAL7::IPC1*, *GAL7::IPC1*+C6 phytoceramide, *GAL7::IPC1*+ C18 ceramide, and *Δcer1* at 37°C, 5% CO_2, pH 4.0. Data are expressed as mean ± SEM.

IPC and GlcCer isoforms, play a major role in regulation of Pma1 and normal cell growth.

DISCUSSION

An understanding of the mechanisms driving *C. neoformans* pathogenicity is an increasingly important area of research because of the growing number of cases of cryptococcosis worldwide. Deeper insight into how this pathogen efficiently maintains itself within immunocompromised hosts will bring us to closer to finding a way to control its growth and dissemination. Dynamic adjustment of the sphingolipid profile in *C. neoformans* cells has been reported to play a significant role in *C. neoformans*'s ability to grow in either highly acidified phagocytic environment or slightly alkaline blood, alveolar, and brain tissue environments. Previous studies attempting to elucidate this pathway have uncovered important pieces of this puzzle (Del Poeta et al., 2015; Rittershaus et al., 2006; Luberto et al., 2001). In the present study, we provide a more comprehensive view of the involved genes and show their importance in the lipid profile switch between these two contrasting environments.

Here, we show that ceramide synthase *Cer1* is a major factor in the pathogenicity of *C. neoformans*. We observed that deletion of each ceramide synthase showed a survival curve that was significantly divergent from WT infection, with *Δcer1* being completely avirulent with 80% of mice totally clearing the infection within 60 days. Lack of *in vitro* growth in host intracellular and extracellular conditions suggests that *Δcer1* lacks the ability to efficiently thrive in the host upon infection. In stark contrast to previous studies on *Δgcs1* and *GAL7::IPC1*, cells of *Δcer1* quickly begin to die when grown in minimal medium conditions regardless of either pH. An inhibitor of *Cer1* could potentially be a very good drug for the treatment of cryptococcosis and other fungal diseases.

There are studies that suggest a role of phytoceramides in the activity of plasma membrane proton pumping H^+-ATPase, Pma1 (Farnoud et al., 2014; Keniya et al., 2013; Soteropoulos et al., 2000). Our results show that *Δcer1* has a marked reduction in the activity of Pma1, thereby suggesting a role, possibly through an indirect mechanism, of C18 ceramides in the ability of *C. neoformans* to maintain its survival within the highly acidic phagolysosome. Increased Pma1 activity in the *Δgcs1* mutant suggests two possible models of ceramide species mediated regulation of Pma1: it is possible that the lack of GlcCer species in *Δgcs1* relieves an inhibitory pressure on Pma1 activity, causing the observed increase. Alternatively, a buildup of intermediate ceramide compounds or IPCs in response to a lack of *Gcs1* (Table S2) could have a positive effect on Pma1 activity, which could also result in the observed increase. Pma1 activity in the presence of AbA and *Δgcs1* indicates intermediate ceramide compounds play a major role in the enzyme's activity.

Δcer1 cells have critical defects in cytokinesis in the presence of host-like environmental stresses. The cell wall is improperly anchored to the plasma membrane in many cells; consequently the membrane and cell wall structure may be inhibiting daughter cell separation. It remains unclear if the altered morphology of the cell wall or the lack of cell wall adherence to the plasma

membrane is the major contributor to this phenotype. The presence of irregular amounts of long-chain ceramides and complex sphingolipids could be affecting the rigidity of the cell wall and/or plasma membrane.

We observed that each knockout strain had distinct alterations of ceramides and downstream lipids, as shown by lipidomic analysis, indicating that the genes are not functionally redundant, and each likely plays a specific role in maintaining the optimum lipid profile for *C. neoformans* membranes. Despite numerous attempts to create a double-mutant *Δcer2Δcer3*, we have been unsuccessful. We suspect, but are unable to confirm because of tight genetic linkage, that the presence of either *Cer2* or *Cer3* is essential to cell survival. Furthermore, the inability of *Δcer1* cells to survive in acidic conditions, despite abundant amounts of IPC-42:0:4, strongly suggests an important role of C18 ceramides for this phenotype.

In summary, this study is a novel insight into the critical importance of ceramides and ceramide synthases in cryptococcal pathogenicity. *Cer1* predominately uses C18 fatty acid chain substrates in order to synthesize specific ceramides and complex sphingolipids that are of crucial importance toward *C. neoformans* pathogenicity. Our results can be extrapolated to several other pathogenic fungi and therefore provide new hope for immunocompromised individuals susceptible to fungal infections.

EXPERIMENTAL PROCEDURES

Strains, Plasmids, and Media

The strains used in this study are *C. neoformans var. grubii* strain H99 as wild-type (WT) and *S. cerevisiae* BY4741. The bacterial strain used was *Escherichia coli* DH5-α Max Efficiency (Invitrogen, Carlsbad, CA, USA) as competent cells. The three putative ceramide synthase genes in this study have the following identifiers: CNAG_06717 (GenBank: XM_012192296), CNAG_02086 (GenBank: XM_012194542), and CNAG_02087 (GenBank: XM_012194543). pYES2/CT was used for overexpression of CNAG_06717 in *S. cerevisiae* BY4741 and pRS425 for CNAG_02086 and CNAG_02087. *C C. neoformans* strains were routinely grown in YPD broth at 30°C and 0.04% CO_2 shaking overnight. DMEM buffered with 25 mM HEPES (pH 4.0 or 7.4) was used to grow *C. neoformans* at 37°C in the presence of 5% CO_2. *S. cerevisiae* transformed with pYES2/CT was grown in YNB (ura^-), and *S. cerevisiae* transformed with pRS425 was grown in synthetic leucine (leu^-) dropout media. Strains containing both vectors were grown in synthetic leu^-ura^- dropout media. Bacterial strains were grown at 37°C in Luria-Bertani media containing 75 mg/L of ampicillin (Sigma-Aldrich). All primers are specified in Table S1.

Phylogenetic Analysis of Putative Ceramide Synthase Genes

Exact maximum likelihood phlyogenetic tree construction was performed using TreePuzzle (Schmidt et al., 2002; Schmidt and Von Haeseler, 2007) with 1,000 quartet puzzling steps. Dendroscope was used to visualize the resulting phylogenetic tree (Huson et al., 2007; Huson and Scornavacca, 2012).

Fluorescent Cryptococcal Ceramide Synthase Assay

An assay for ceramide synthase activity was adapted (Kim et al., 2012; Tidhar et al., 2015) with minor changes. Enzymes were extracted as microsomes (see Supplemental Experimental Procedures). Reactions contain 10 μM NBD-sphingosine or NBD-phytosphingosine (Avanti Polar Lipids) and 50 μM fatty acyl CoA (C18, C24, C26) (Avanti Polar Lipids, Alabaster, AL, USA). One hundred fifty micrograms of microsomal protein was added per reaction. Reactions were incubated at 35°C for 90 min, followed by enzyme inactivation with 2:1 chloroform/methanol. The lipids were extracted and dried in a SpeedVac (SPD 2010; Thermo Fisher Scientific) and resuspended in 100% methanol. The reaction was analyzed using thin-layer chromatography, using chloroform/methanol/water (8:1:0.1, v/v/v) as the solvent mixture.

Virulence Studies and Histology Analysis in a Murine Mouse Model of Cryptococcosis

Three- to 4-week-old female CBA/JCrHsd mice (Harlan Laboratories) were used for all experiments. Mice were infected with WT, Δ*cer1*, Δ*cer2*, Δ*cer3*, and Δ*cer1*+*CER1* at a concentration of 3.5×10^7 cells/mL. For survival studies, ten CBA/JCrHsd mice per strain were infected intranasally with 7×10^5 cells/20 μL. For tissue burden analysis, nine mice per strain were used. Organs were excised and homogenized in 10 mL PBS using Stomacher 80 (Seward) for 2 min at high speed. For histopathology analysis, three mice per experimental group were used. Mice organs were fixed in 3.7% formaldehyde in paraffin and stained with H&E and mucicarmine. All animal procedures were approved by the Stony Brook University Institutional Animal Care and Use Committee and followed the guidelines of American Veterinary Medical Association.

Extraction and Mass Spectrometry Analysis of Yeast Sphingolipids

Lipid extraction was performed according to the methods of Bligh and Dyer (1959). After measuring the dry weights, the samples were subject to base hydrolysis (Clarke and Dawson, 1981). The extracts were dried in a SpeedVac (SPD 2010, ThermoFisher Scientific, Waltham, MA, USA). All internal standards were added prior to lipid extraction. Mass spectrometry (MS) analysis detailed in Supplemental Experimental Procedures.

In Vitro Growth Studies

Cells of *C. neoformans* WT, Δ*cer1*, and Δ*cer1*+*CER1* were grown in 10 mL DMEM (buffered with HEPES [pH 4.0 or 7.4]) to a final density of 10^4 cells/mL and incubated in shaker incubator at 37°C with 5% CO_2 or YPD (30°C, 0.04% CO_2) where mentioned. *GAL7::IPC1* was grown as previously described (Luberto et al., 2001). Aliquots were taken at the time points indicated. For cell wall stability, cells were spotted in serial dilutions on YPD plates with 0.05% SDS. For oxidative stress, cells were spotted on YPD containing 2 mM H_2O_2. C6 phytoceramide (50 μM) (Matreya) and C18 ceramide (Avanti Polar Lipids) were supplemented where mentioned.

Transmission Electron Microscopy

C. neoformans strains were grown for 24 hr in DMEM (pH 4.0 or 7.4) at 37°C + 5% CO_2. Cells were later washed and fixed in 3% EM-grade glutaraldehyde solution for 2 hr. Cells were supplemented with 50 μM ceramide mix where indicated (Matreya). (Additional sample preparation details are provided in Supplemental Experimental Procedures.) Visualization of samples was performed using a FEI TeCnai12 BioTwinG^2 transmission electron microscope. Digital images were acquired with an AMT XR-60 charge-coupled device (CCD) digital camera system.

Glucose-Dependent Medium Acidification to Measure Plasma Membrane H^+-ATPase

Glucose-dependent medium acidification was monitored by a modification of a procedure described previously (Perlin et al., 1988; Soteropoulos et al., 2000). Briefly, cells of WT, *Δcer1*, *Δcer1*+*CER1*, and *Δgcs1* were grown to mid-log phase in YPD. The following day, cells were transferred to DMEM at pH 4.0 for 24 hr. AbA (0.05 μg/mL) and 50 μM ceramide supplements were added where mentioned. Cells were then harvested, washed, and resuspended in 100 mM KCl (pH 5.0), shaking at 30°C for 1 hr. These samples were then stored at 4°C overnight prior to use. For the assay, cells were concentrated to a final A590 of approximately 2.0. Twenty microliters of cells along with 155 μL of bromophenol blue (50 μg/mL) in 100 mM KCl (pH 5.0) and 20 μL 20% (w/v) glucose was added to initiate the reaction. Medium acidification was monitored at 590 nm over a period of 5 hr (data point every 3 mins) in a microplate reader (SpectraMax M5)

Statistics

Data are expressed as mean ± SEM. Calculations were made and data graphed using GraphPad Prism software version 6.0.

SUPPLEMENTAL INFORMATION

Supplemental Information includes Supplemental Experimental Procedures, five figures, three tables, and one data file and can be found with this article online at https://doi.org/10.1016/j.celrep.2018.01.035.

ACKNOWLEDGMENTS

This work was supported by NIH grants AI116420 and AI125770 to M.D.P. and AI127704 to B.C.F. and in part by National Cancer Institute (NCI) grant P01-CA97132 to C.L. for project #4. M.D.P. is a Burroughs Welcome Investigator in Infectious Diseases. We are grateful to Dr. Martha Furie, Dr. Jamie Konopka, Dr. Luis Martinez, Dr. Amir Farnoud, Dr. Visesato Mor, Dr. Aaron Neiman, and members of the Del Poeta and Luberto labs for valuable inputs. Special thanks to Dr. Can Senkal for providing mammalian *CER1* microsomes. We thank Susan Van Horn and the transmission electron microscopy (TEM) facility at the Central Microscopy Imaging Center (C-MIC) at Stony Brook University. We thank Yelena Altschuller for help with plasmid construction. The Stony Brook Proteomics facility, Research Histology core, and the McClain lab provided valuable assistance for several experimental procedures. We thank Jasna Boudard and Zoe Reifsnyder for their help with graphics and figures.

AUTHOR CONTRIBUTIONS

Conceptualization, M.A.M., J.M.G., C.L., and M.D.P.; Methodology, M.A.M. and J.M.G.; Investigation, M.A.M.; Lipidomics, A.S. and R.R.; Writing – Original Draft, M.M. and J.M.G.; Writing – Review & Editing, J.M.G. and M.D.P.; Replicative Lifespan Study, T.B. and B.C.F.; Funding Acquisition, Resources, and Supervision, M.D.P.

DECLARATION OF INTERESTS

M.D.P. is a co-founder and chief scientific officer (CSO) of MicroRid Technologies. All other authors have no conflict of interest.

Received: September 29, 2017
Revised: December 2, 2017
Accepted: January 11, 2018
Published: February 6, 2018

REFERENCES

Aguilera-Romero, A., Gehin, C., and Riezman, H. (2014). Sphingolipid homeostasis in the web of metabolic routes. Biochim. Biophys. Acta *1841*, 647–656.

Alvarez, M., and Casadevall, A. (2006). Phagosome extrusion and host-cell survival after Cryptococcus neoformans phagocytosis by macrophages. Curr. Biol. *16*, 2161–2165.

Bligh, E.G., and Dyer, W.J. (1959). A rapid method of total lipid extraction and purification. Can. J. Biochem. Physiol. *37*, 911–917.

Cheon, S.A., Bal, J., Song, Y., Hwang, H.M., Kim, A.R., Kang, W.K., Kang, H.A., Hannibal-Bach, H.K., Knudsen, J., Ejsing, C.S., and Kim, J.Y. (2012). Distinct roles of two ceramide synthases, CaLag1p and CaLac1p, in the morphogenesis of Candida albicans. Mol. Microbiol. *83*, 728–745.

Clarke, N.G., and Dawson, R.M. (1981). Alkaline O leads to N-transacylation. A new method for the quantitative deacylation of phospholipids. Biochem. J. *195*, 301–306.

Del Poeta, M., Nimrichter, L., Rodrigues, M.L., and Luberto, C. (2015). Correction: synthesis and biological properties of fungal glucosylceramide. PLoS Pathog. *11*, e1004886.

Farnoud, A.M., Mor, V., Singh, A., and Del Poeta, M. (2014). Inositol phosphosphingolipid phospholipase C1 regulates plasma membrane ATPase (Pma1) stability in Cryptococcus neoformans. FEBS Lett. *588*, 3932–3938.

Feldmesser, M., Kress, Y., Novikoff, P., and Casadevall, A. (2000). Cryptococcus neoformans is a facultative intracellular pathogen in murine pulmonary infection. Infect. Immun. *68*, 4225–4237.

Huson, D.H., and Scornavacca, C. (2012). Dendroscope 3: an interactive tool for rooted phylogenetic trees and networks. Syst. Biol. *61*, 1061–1067.

Huson, D.H., Richter, D.C., Rausch, C., Dezulian, T., Franz, M., and Rupp, R. (2007). Dendroscope: an interactive viewer for large phylogenetic trees. BMC Bioinformatics *8*, 460.

Kageyama-Yahara, N., and Riezman, H. (2006). Transmembrane topology of ceramide synthase in yeast. Biochem. J. *398*, 585–593.

Keniya, M.V., Cannon, R.D., Nguyễn, Â., Tyndall, J.D., and Monk, B.C. (2013). Heterologous expression of Candida albicans Pma1p in Saccharomyces cerevisiae. FEMS Yeast Res. *13*, 302–311.

Kim, H.J., Qiao, Q., Toop, H.D., Morris, J.C., and Don, A.S. (2012). A fluorescent assay for ceramide synthase activity. J. Lipid Res. *53*, 1701–1707.

Li, S., Du, L., Yuen, G., and Harris, S.D. (2006). Distinct ceramide synthases regulate polarized growth in the filamentous fungus Aspergillus nidulans. Mol. Biol. Cell *17*, 1218–1227.

Luberto, C., Toffaletti, D.L., Wills, E.A., Tucker, S.C., Casadevall, A., Perfect, J.R., Hannun, Y.A., and Del Poeta, M. (2001). Roles for inositol-phosphoryl ceramide synthase 1 (IPC1) in pathogenesis of C. neoformans. Genes Dev. *15*, 201–212.

Perlin, D.S., Brown, C.L., and Haber, J.E. (1988). Membrane potential defect in hygromycin B-resistant pma1 mutants of Saccharomyces cerevisiae. J. Biol. Chem. *263*, 18118–18122.

Rajasingham, R., Smith, R.M., Park, B.J., Jarvis, J.N., Govender, N.P., Chiller, T.M., Denning, D.W., Loyse, A., and Boulware, D.R. (2017). Global burden of disease of HIV-associated cryptococcal meningitis: an updated analysis. Lancet Infect. Dis. *17*, 873–881.

Rittenour, W.R., Chen, M., Cahoon, E.B., and Harris, S.D. (2011). Control of glucosylceramide production and morphogenesis by the Bar1 ceramide synthase in Fusarium graminearum. PLoS ONE *6*, e19385.

Rittershaus, P.C., Kechichian, T.B., Allegood, J.C., Merrill, A.H., Jr., Hennig, M., Luberto, C., and Del Poeta, M. (2006). Glucosylceramide synthase is an essential regulator of pathogenicity of Cryptococcus neoformans. J. Clin. Invest. *116*, 1651–1659.

Schmidt, H.A., and Von Haeseler, A. (2007). Maximum-likelihood analysis using TREE-PUZZLE. Curr. Protoc. Bioinformatics. *Chapter 6*, Unit 6.6.

Schmidt, H.A., Strimmer, K., Vingron, M., and von Haeseler, A. (2002). TREE-PUZZLE: maximum likelihood phylogenetic analysis using quartets and parallel computing. Bioinformatics *18*, 502–504.

Singh, A., and Del Poeta, M. (2011). Lipid signalling in pathogenic fungi. Cell. Microbiol. *13*, 177–185.

Soteropoulos, P., Vaz, T., Santangelo, R., Paderu, P., Huang, D.Y., Tamás, M.J., and Perlin, D.S. (2000). Molecular characterization of the plasma membrane H(+)-ATPase, an antifungal target in Cryptococcus neoformans. Antimicrob. Agents Chemother. *44*, 2349–2355.

Ternes, P., Wobbe, T., Schwarz, M., Albrecht, S., Feussner, K., Riezman, I., Cregg, J.M., Heinz, E., Riezman, H., Feussner, I., and Warnecke, D. (2011). Two pathways of sphingolipid biosynthesis are separated in the yeast Pichia pastoris. J. Biol. Chem. *286*, 11401–11414.

Tidhar, R., Sims, K., Rosenfeld-Gur, E., Shaw, W., and Futerman, A.H. (2015). A rapid ceramide synthase activity using NBD-sphinganine and solid phase extraction. J. Lipid Res. *56*, 193–199.

Cell Reports, Volume *22*

Supplemental Information

The Role of Ceramide Synthases in the Pathogenicity of *Cryptococcus neoformans*

Mansa A. Munshi, Justin M. Gardin, Ashutosh Singh, Chiara Luberto, Robert Rieger, Tejas Bouklas, Bettina C. Fries, and Maurizio Del Poeta

Supplemental information:

Supplementary Figures:

Figure S1 [Deletion and reconstitution of the *Cn* Cer1/Cer2/Cer3 gene, and alignment of fungal and mammalian ceramide synthases], Related to Figures 1,2,3,4,5 :

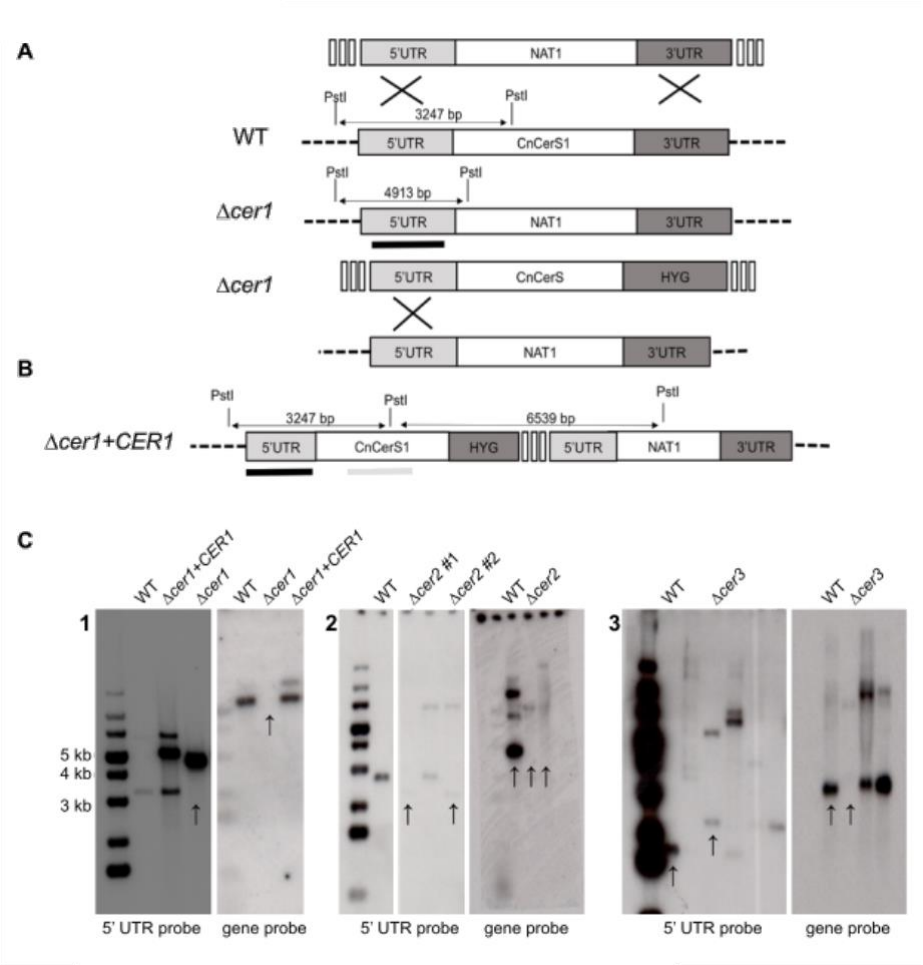

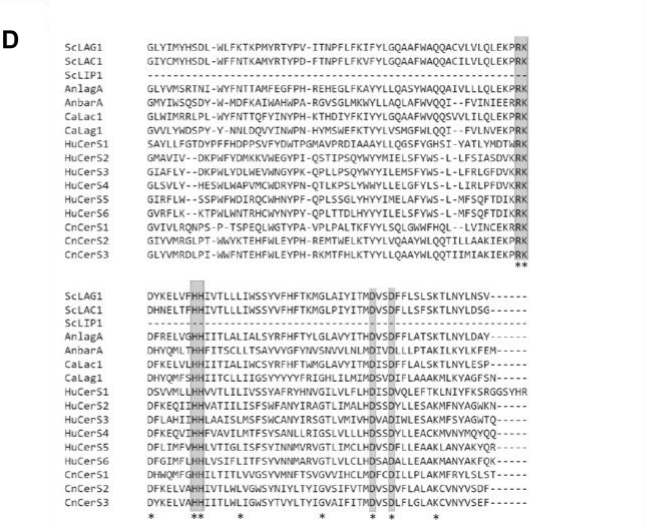

Supplementary figure 1: Deletion and reconstitution of the *Cn* Cer1/Cer2/Cer3 gene: (A) General strategy for the deletion of ceramide synthases in *C. neoformans* wild-type (WT) and creation of the mutant strain *Δcer*. (B) Strategy for the generation of the complemented strain *Δcer+CER*.

(C) Southern blot analysis for confirmation of transformants of *Δcer1, Δcer2 and Δcer3*.

Lanes: 1-4 5'UTR probe for *Δcer1*. Lane 1- 1kb marker, lane 2-WT *Cn*, lane 3- *Δcer1+CER1*, lane 4- *Δcer1*. Lanes (6-8) gene probe for *Δcer1* selection. 6-WT, 7- *Δcer1*, 8- *Δcer1+CER1*. Lane (9-16) 5'UTR and gene probes for *Δcer2*. 9-1 kb marker, 10-WT band, 11, 13- *Δcer2* transformants, 12-WT band. Lanes (17-23) 5'UTR and gene probes for *Δcer3*. 17-1 kb marker, 18-WT band, 19- *Δcer3*, 20-WT, 21- *Δcer3*, 22, 23- negative transformants.

5' UTR, 5' untranslated region; 3' UTR, 3' untranslated region; NAT1, nourseothricin 1; Cer1, ceramide synthase1 1; HYG. Hygromycin B.

(D) Alignment of amino acid sequences of fungal and human ceramide synthases using Clustal Omega algorithm '*' indicated conserved residues. Grey boxes are conserved residues that have been reported to be important for ceramide synthase activity. *Sc, S.cereviaise; Ca, C.albicans; An, A. nidulans; Hu, Homo sapiens; Cn, C. neoformans*. Related to Figure 1

Figure S2 [Histopathology of Brain and lung sections of mice infected intranasally], Related to Figure 2:

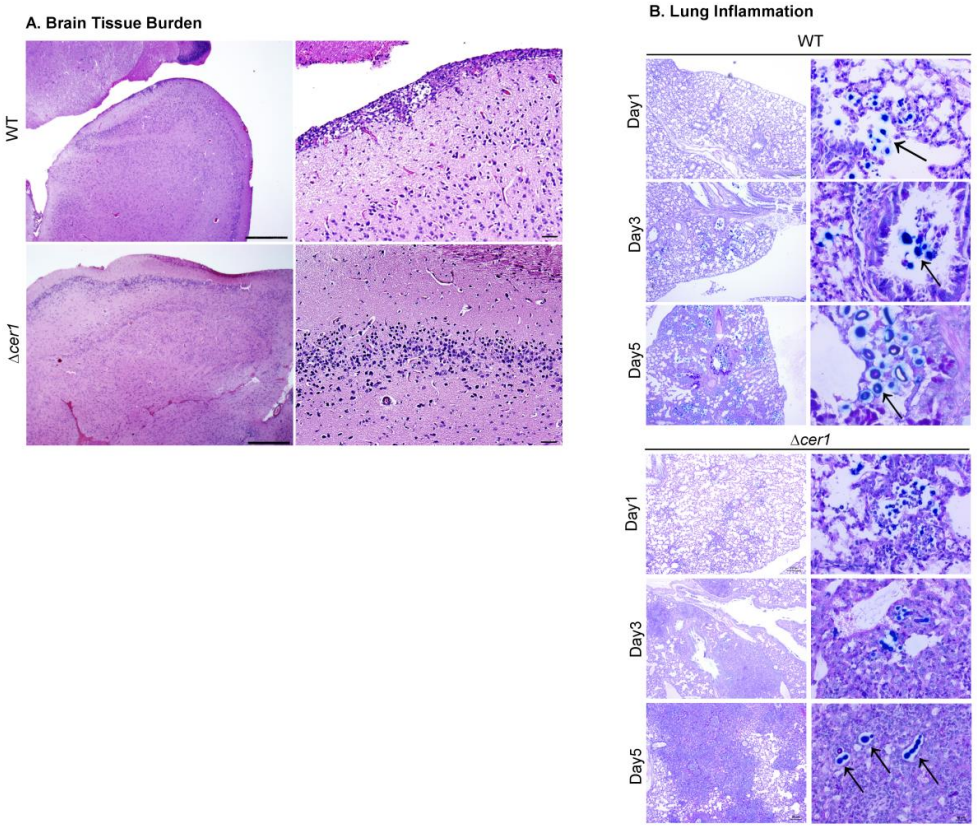

Supplementary figure 2: (A) Histopathology of Brain sections of mice infected intranasally with WT (at death) or *Δcer1* (day 60). Sections stained with haematoxylin & Eosin. Bar=1mm (left), 100µm (right) (B) Histopathology of lungs obtained from CBA/J mice infected intranasally with wildtype (WT) or *Δcer1* at days 1,3 and 5 post infection. Infection with WT *Cn* shows a progression of inflammation along with replication of cells from day 1-5. Infection with Δ*cer1* shows a reduction in the number of cells from day 1-5 and cells start showing an elongated phenotype within 24-48 hours in the lung. Inflammation is observed during this time. Sections stained with Periodic acid Schiff's stain/Alcian Blue and Haematoxylin. Bar = 20µm. Black arrows show *Cn* cells**.**

Figure S3 [Expression of Cer1 in *S. cerevisiae*], Related to Figure 1B:

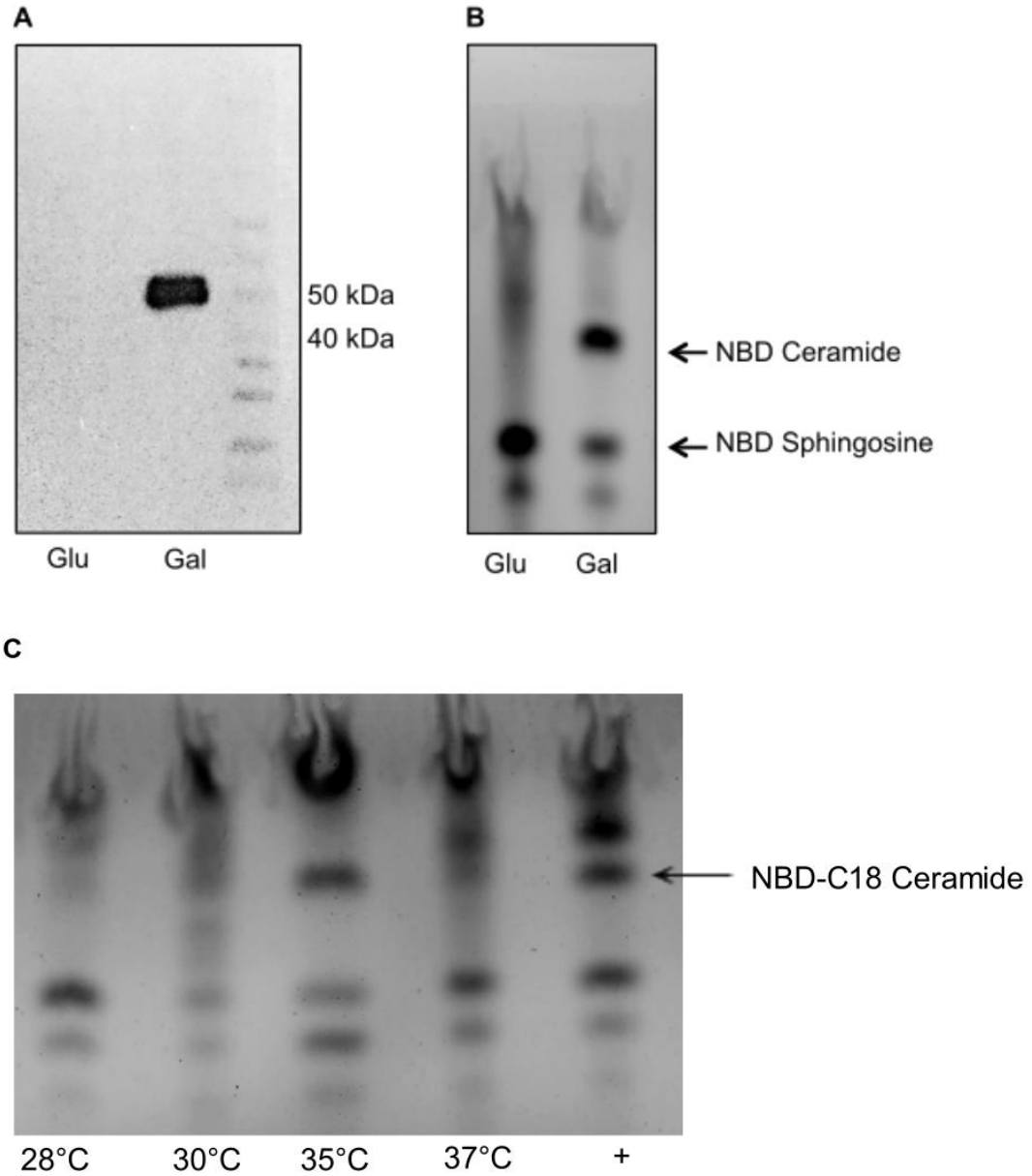

Supplementary figure 3: Expression of Cer1 in *S. cerevisiae*

(A) Western blot using microsomal protein from Cer1 expressed in 2% glucose or 2% galactose. using anti-6XHis antibody. 150µg microsomal protein was used in each lane.

(B) Ceramide synthase assay confirming activity of Cer1 in *Sc*. 150µg microsomal protein was used in each lane.

(C) Cer1 activity is temperature dependent. Ceramide synthase assay using 150µg microsomal protein of Cer1 at temperature 28℃, 30℃, 35℃, and 37℃. Formation of NBD-ceramide was detected by thin layer chromatography. Mammalian Cer1 microsomal protein was used as a positive control.

Figure S4 [Heat map of the sphingolipid profile for ceramide synthase deletion strains], Related to Figure 3:

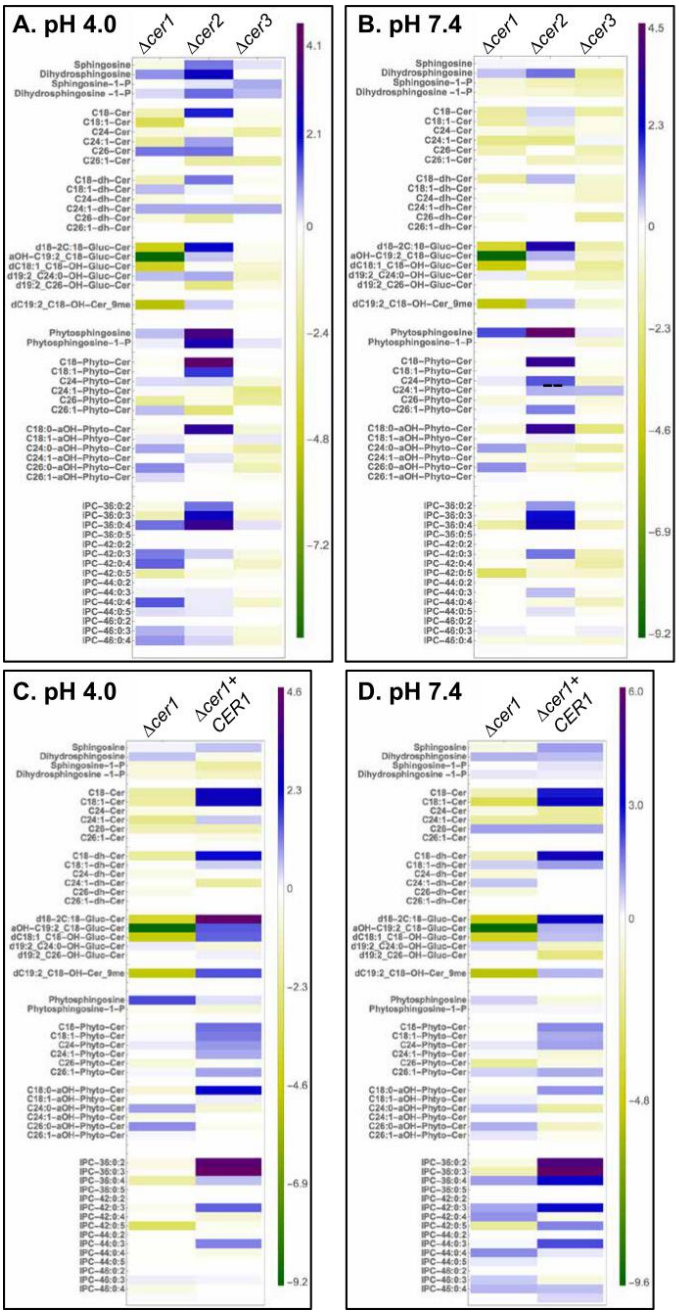

Supplementary figure 4: Heat map of the sphingolipid profile for ceramide synthase deletion strains. The amount of lipid species are represented as relative abundance to corresponding WT lipid values. Blue bars represent lipid amount higher than WT. Green bars represent amount of lipid lower than WT. White bars are equal to WT values.

A. Lipid profile at pH 4.0/intracellular conditions.

B. Lipid profile at pH 7.4/extracellular conditions. The scale is $\log_2$.

(C & D) Heat map of the sphingolipid profile for Δ*cer1*, and Δ*cer1 +CER1* strains

C. Lipid profile at pH 4.0/intracellular conditions.

D. Lipid profile at pH 7.4/ extracellular conditions. The scale is log_2.

Figure S5 [Replicative lifespan studies for WT, Δ*cer1*, and Δ*cer1 +CER1*], Related to Figure

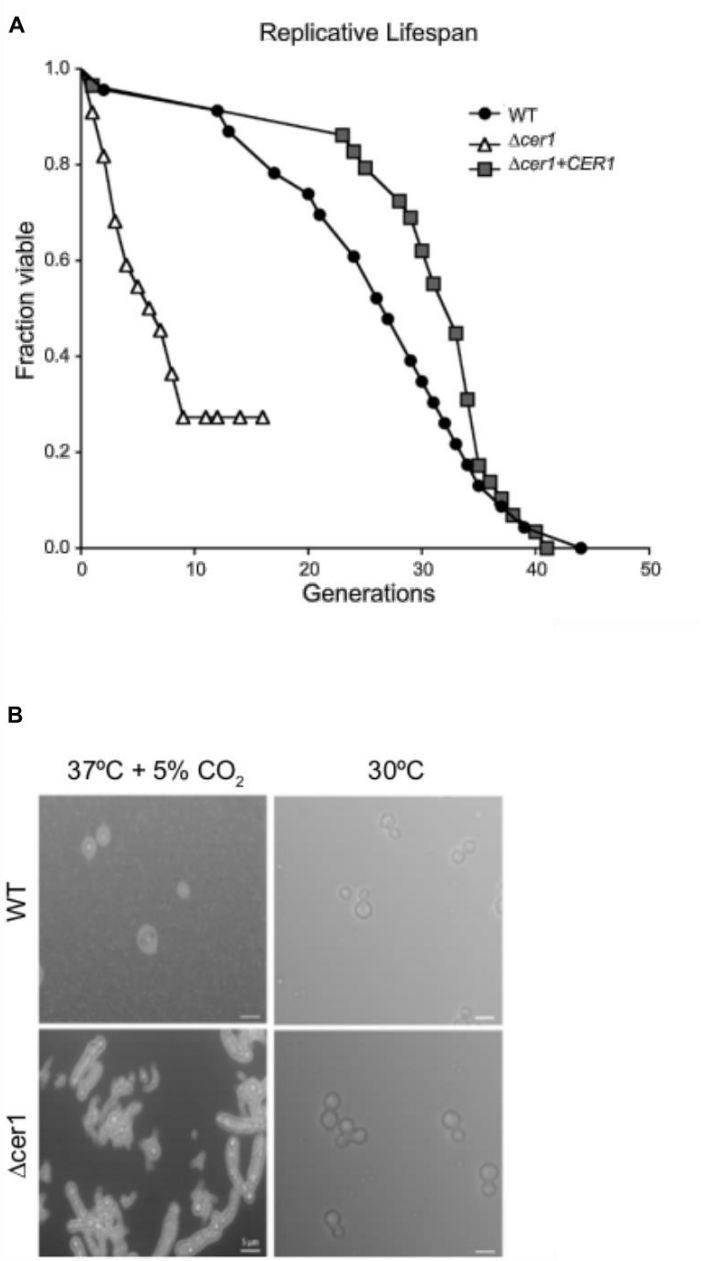

Supplementary figure 5 (A) Replicative lifespan studies for WT, Δ*cer1*, and Δ*cer1 +CER1* shows that deletion of Cer1 leads to a drastic reduction of lifespan to an average 6.5 generations. While WT and Δ*cer1 +CER1* has a lifespan of average 27 generations.

(B) Light microscopy reveals cell wall defects in Δ*cer1*.

India ink staining shows that Δ*cer1* undergoes abnormal budding when exposed to physiological conditions. Cells of Δ*cer1* show an elongated phenotype as an outcome of incomplete cell division. These cells appear similar to WT at 30℃ and rich media.

Table S1: Primers used in this study. Related to experimental procedures:

Number	Name	Sequence 5'-3'
1	CNAG_067175UTRF	CTGGATCCGCGTCAAGTGGGTATTTCGT
2	CNAG_067175UTRR	CTACTAGTAGCTCGTGGGTGTTTGGTTA
3	CNAG_067173UTRF	CTGATATCTCTTGGATAGCCTGCGACTT
4	CNAG_067173UTRR	CTGGGCCCGACGTCAGGAAGCCTTTGTC
5	CNAG_0202865UTRF	CTGGATCCGGCCGTGAAGAGGAATAACA
6	CNAG_020865UTRR	CTACTAGTGTTGTCGAGATGTGGCTGAA
7	CNAG_020863UTRF	CTCTCGAGGGTGATCGTGGCTTGCTT
8	CNAG_020863UTRR	CTGGGCCCTAGCTGTTCTACGTCAAGTGGTC
9	CNAG_020875UTRF	CTGGATCCGGTGATCGTGGCTTGCTT
10	CNAG_020875UTRR	CTACTAGTTAGCTGTTCTACGTCAAGTGGTC
11	CNAG_020873UTRF	CTCTCGAGCAGGTGATGCACCGTGAGA
12	CNAG_020873UTRR	CTGGGCCCGAAGGACCTTTCCCAACTCC
13	pRS425_Ahomo_gal1p	ccctcgaggtcgacggtatcgataagcttgatatcgaattcctgcagccc GATCCACTAGTACGGATTAGAAGCC
14	pYES/ct_86homo	GACCTTCGCCGATGGCTGGGCTTATTTGGTGTCACTGCTGGAC CGGGCAT GTTTTTTCTCCTTGACGTTAAAGTATAGAG
15	pYES/ct_87homo	GTTACACTGGACGCTCGCCTTCGGTGAAGATGTTTATGCCTTT GGGACAT GTTTTTTCTCCTTGACGTTAAAGTATAGAG
16	86_ATG_fwd	ATGCCCGGTCCAGCAGTG
17	87_ATG_fwd	ATGTCCCAAAGGCATAAACATCTTC

18	86_TAA_pRS425Homo	agctggagctccaccgcggtggcggccgctctagaactagtggatccccc TTACTCAGCCTTCACCTTCACTTC
19	87_TGA_pRS425Homo	agctggagctccaccgcggtggcggccgctctagaactagtggatccccc TCATTCTTCCTTCGCTTCATCC
20	IDTMMREC67F	ACATCACACTGCGGCCTCATCGTGCCTCTCCTTTTC
21	IDTMMREC67R	GTCAAGCTAAGCGGCCCAAGTCGCAGGCTATCCAA
22	MMREC86F	ACATCACACTGCGGCCGCGGCCGTGAAGAGGAATAACA
23	MMREC86R	GTCAAGCTAAGCGGCCGCCGGAAACATCACTCAAGCAA
24	MMREC87F	ACATCACACTGCGGCCGCGTGATCGTGGCTTGCTTGAG
25	MMREC87R	GTCAAGCTAAGCGGCCGCCTATCCGTCTACTGAACGATTA

Table S2. Lipid species composition of SL biosynthetic pathway mutants. Related to Figure 3, 5

Lipid species	*Cn* WT	*Δgcs1*	*GAL7::IPC1*	*Δcer1*	*Δcer2*	*Δcer3*
C18 Ceramide species	680.95	6037.44	1082.24	9.82	443.3	674.97
α-OH-Δ4-Δ8, 9Me-GlcCer	3105.48	0.00	12823.82	4.96	1685.93	2821.22
Phyto-Sph	0.16	0.04	0.38	0.34	3.34	0.50
Phyto-Sph-1P	0.17	0.21	0.22	0.18	0.05	0.33
PhytoC6	0.02	0.65	0.96	0.16	0.12	0.18
PhytoC14-Cer	0.18	0.25	0.85	0.69	4.16	1.20
PhytoC16-Cer	43.19	238.22	45.56	13.66	209.03	48.89
PhytoC18:1-Cer	178.33	190.04	120.55	9.51	98.66	188.16
PhytoC18-Cer	754.08	3245.00	121.75	17.37	569.30	541.11
PhytoC20:1-Cer	5.54	1.34	4.02	4.33	124.60	4.36
PhytoC20-Cer	8.84	11.69	2.95	5.37	94.65	5.25

PhytoC22:1-Cer	0.98	2.73	0.88	0.48	11.49	0.71
PhytoC22-Cer	44.25	10.79	17.04	21.34	67.46	12.64
PhytoC24:1-Cer	2.28	1.92	4.27	5.15	2.34	1.47
PhytoC24-Cer	583.66	136.33	260.58	667.00	742.17	350.59
PhytoC26:1-Cer	59.04	12.34	33.44	45.23	54.57	38.60
PhytoC26-Cer	86.78	34.83	41.82	119.93	284.50	57.28
PhytoC28:1-Cer	9.02	4.08	4.37	7.78	24.26	10.00
PhytoC28-Cer	4.78	5.32	6.03	3.58	19.37	3.93
αOH-PhytoC14-Cer	302.47	8.04	25.19	4.44	11.47	6.39
αOH-PhytoC16-Cer	9.61	0.00	0.00	0.00	0.00	0.00
αOH-PhytoC18:1-Cer	9.16	0.00	1.93	0.08	1.41	0.94
αOH-PhytoC18-Cer	111.05	98.39	185.51	65.06	623.64	90.02
αOH-PhytoC20:1-Cer	15.00	0.00	0.16	0.00	0.72	0.12
αOH-PhytoC20-Cer	29.65	30.15	31.78	20.74	42.00	19.00
αOH-PhytoC22:1-Cer	1.45	0.00	0.00	0.05	0.00	0.00
αOH-PhytoC22-Cer	67.94	91.14	65.80	62.26	92.91	42.93
αOH-PhytoC24:1-Cer	0.00	0.71	0.00	0.00	2.99	0.53
αOH-PhytoC24-Cer	2456.35	2217.29	4060.07	2796.37	1192.94	1391.92
αOH-PhytoC26:1-Cer	0.00	0.19	0.00	1.66	1.34	0.34
αOH-PhytoC26-Cer	125.07	115.01	266.64	348.00	165.48	90.21
αOH-PhytoC28:1-Cer	0.00	0.09	0.00	0.06	0.00	0.00
αOH-PhytoC28-Cer	0.00	0.03	0.00	0.02	0.00	0.00

Table 2:

Lipid abundance in WT, Δ*gcs1, GAL7::IPC1,* Δ*cer1,* Δ*cer2,* and Δ*cer3* strains measured by LC-MS. Strains were grown in YNB, 2% glucose before extracting lipids (see methods). C18 ceramide species include: α-OH-Δ4-ceramide, α-OH-Δ4-Δ8 ceramide, and α-OH-Δ4-Δ8, 9Me ceramide. All concentrations are represented as pmol/mg dry lipid weight.

Table S3: C18 ceramide abundance of *GAL7::IPC1* at 6 hours, 12 hours, 24 hours and 48 hours post glucose inoculation. Related to Figure 5

Time	WT pH 4.0	*GAL7::IPC1 pH 4.0*	WT pH 7.0	*GAL7::IPC1 pH 7.0*
6 hours	23.93	10.90	18.64	6.49
12 hours	31.80	3.152	30.46	0.043
24 hours	11.46	37.534	18.41	6.90
48 hours	20.53	34.64	25.473	8.59

Table 3: C18 ceramide changes of WT and *GAL7::IPC1* upon glucose transfer. When Ipc1 is genetically downregulated, a transient decrease is observed in C18 ceramide levels because cells do not tolerate high levels of ceramides. As the cells start to adapt, growth is restored likely due to a parallel increase in C18 ceramides. These C18 ceramides then lead to an increase in GlcCer which is highly abundant in *GAL7::IPC1* at 48 hours post glucose inoculation (Supplementary table 2).

WT and *GAL7::IPC1* were grown overnight in galactose containing media. Strains were transferred to glucose media after 16-22 hours and samples were collected for lipid analysis at mentioned time points. Lipid extraction and analysis was performed as mentioned in the methods. Values represented as pmol/mg dry lipid weight.

Experimental procedures

Strains, Plasmids and Media

The strains used in this study are *Cryptococcus neoformans var. grubii* strain H99 as wildtype (WT) and *S. cerevisiae* BY4741. Bacterial strain used was Escherichia coli DH5-α™ Max Efficiency® (Invitrogen, Carlsbad, CA) as competent cells. Plasmid pCR topo 2.1 was used for cloning and biolistic transformation. Cloning was carried out using TOPO® TA Cloning® Kit, with pCR™2.1-TOPO® (Invitrogen, Carlsbad, CA). The three putative ceramide synthase genes in this study have the following identifiers: CNAG_06717 (Genbank accession number XM_012192296), CNAG_02086 (Genbank accession number XM_012194542), CNAG_02087 (Genbank accession number XM_012194543). For overexpression studies, pYES2/CT was used for expression of CNAG_06717 in *S.cerevisiae* BY4741 while pRS425 was used to express CNAG_02086 and CNAG_02087. *Cn* strains were routinely grown in YPD broth at 30°C and 0.04% CO_2 for 20-22 hours with shaking at 225 rpm. Dulbecco's

modified eagle medium (DMEM) buffered with 25mM HEPES (pH 4.0 or pH 7.4) was used to grow *Cn* at 37°C in the presence of 5% CO_2 (physiologically relevant conditions). *S. cerevisiae* transformed with pYES2/CT was grown in YNB without amino acids, 1g/L amino acid mixture lacking uracil (ura^-), 5g Ammonium sulfate, 0.4g $NaPO_4$ dibasic, and 2% Glucose or 1% Galactose + 1% Raffinose (to induce expression). Similarly, *S. cerevisiae* transformed with pRS425 was grown in synthetic leucine (leu^-) dropout media. Strains containing both vectors were grown in synthetic leu^-ura^- dropout media. Bacterial strains were grown at 37°C in Luria–Bertani media containing 75mg/L of ampicillin (Sigma).

Isolation and cloning of *C. neoformans* ceramide synthase genes

To independently delete each of the three ceramide synthase genes from the genome of *C. neoformans*, plasmids using nourseothricin acetyltransferase (NAT1) (Werner BioAgents, Germany) selectable marker deletion strategy were constructed. Each NAT1 deletion plasmid contained 1.5 kilobases (Kb) of 5' untranslated region (UTR) upstream of the ORF as well as 1.5 kilobases of the 3'UTR downstream of the ORF. Generally, the 5'UTR and 3'UTR of the gene of interest was constructed flanking NAT1 gene, whose expression is under the control of actin promoter. The 5'UTR and 3'UTR were generated by PCR using specific primers containing restriction sites on genomic *C. neoformans* H99 DNA. These fragments were then cloned into pCR2.1 TOPO vector generating plasmids pCR-5UTR and pCR-3UTR and sequenced for each of the three genes of interest (Cer1- 5'UTR, Cer1-3'UTR, Cer2- 5'UTR, Cer2-3'UTR. Cer3-5'UTR, Cer3-3'UTR). The 3'UTR was then sub-cloned into plasmid pCR-NAT1 vector, generating plasmid pCR-3UTR:NAT1. The 5'UTR was subcloned into pCR-3'UTR::NAT1 generating pCR 5'UTR::NAT1::3'UTR for each ceramide synthase. These constructs were named pΔcer1, pΔcer2, and pΔcer3. *C. neoformans* wildtype strain H99 was independently transformed with each of the three constructs *pΔcer1, pΔcer2*, and *pΔcer3*, by biolistic transformation according to (Singh, Qureshi et al. 2011). Transformants were grown on Yeast peptone dextrose (YPD) plates containing 100 µg/ml of nourseothricin. Resistant colonies were chosen randomly and purified through serial passage on selective media. Correct integration of DNA cassettes was examined by southern blot analysis and performed according to (Singh, Qureshi et al. 2011). Transformants for each ceramide synthase gene, showing deletion of the gene and insertion of the plasmid cassette were obtained and were chosen and designated Δcer1 strain, Δcer2 strain, and Δcer3 strain. To reintroduce the genes back in their respective knockout mutants, reconstituted constructs, pCR-Cer1-ACT-HYG, pCR-Cer2-ACT-HYG, pCR-Cer3-ACT-HYG plasmid constructs were generated as follows: A fragment (4.5 kb) containing the entire ORF of the gene and 1.5 kb of the upstream (5'UTR) was generated by PCR using wildtype H99 genomic DNA as a template and

was cloned into the pCR2.1-TOPO vector generating plasmid containing 5'UTR –GENE. This construct was then sub cloned into pSK-ACTIN-HYG plasmid containing Hygromycin resistant marker forming pSK-Cer1-ACT-HYG, pSK-Cer2-ACT-HYG, pSK-Cer3-ACT-HYG. The Δ*cer1,* Δ*cer2,* and Δ*cer3* mutant strains were each transformed with pSK-Cer1-ACT-HYG, pSK-Cer2-ACT-HYG, and pSK-Cer3-ACT-HYG plasmid respectively using biolistic delivery of DNA using the scheme as shown (Supp. Fig 1). Transformants were grown on YPD plates containing 100 µg/ml of hygromycin B. Stable transformants were selected, grown on YPD, followed by extraction of DNA and confirmation with southern blot using gene sequence probes. These reconstituted strains were named *Δcer1+CER1, Δcer2+CER2,* and *Δcer3+CER3*.

Phylogenetic analysis of putative ceramide synthase genes

Representative fungal ceramide synthase genes and the three computationally annotated ceramide synthase genes were aligned with ClustalOmega using default parameters. Exact maximum likelihood phlyogentic tree construction was performed using TreePuzzle (Schmidt, Strimmer et al. 2002, Schmidt and von Haeseler 2007) with 1000 quartet puzzling steps. Human ceramide synthase 1 was selected as the outgroup, with the exact neighbor-joining tree method used to find the parameter estimates. The Meuller-Vingron model of substitution was used to calculate mismatch penalties. Dendroscope (Huson, Richter et al. 2007, Huson and Scornavacca 2012) was used to visualize the resulting phylogenetic tree.

Biochemical characterization of *Cn* ceramide synthases

Cn ceramide synthase enzymes were further biochemically characterized using a fluorescent assay using different combinations of substrates and buffer pH. Specifically, NBD-sphingosine, NBD-phytosphingosine were used to check for formation of ceramides and phytoceramides. Fatty Acyl CoA chain lengths C18, C24 and C26 were used tested for chain length specificity. pH dependence of ceramide synthase activity was assessed by using a range of buffers from 3.0-10.0. For all further assays, three buffers: Sodium acetate trihydrate, $CH_3COONa \bullet 3H_2O$, Acetic acid NaOAc buffer (pH 4.0), $Na_2HPO_4 – NaH_2PO_4$ (pH 7.0) and Sodium Carbonate $Na_2CO_3 \bullet 10H_2O$ – Sodium Bicarbonate $NaHCO_3$ (pH 10.0) were used.

Generation of *S. cerevisiae* strains expressing *Cn* ceramide synthases

3 plasmids were constructed respectively for the genes CNAG_06717, CNAG_02086 and CNAG_02087. Gene fragment for CNAG_06717 containing V5 and 6X histidine tags and overlapping ends with pYES2/CT vector was

generated using IDT gblocks gene fragments. The construct was inserted into vector pYES2/CT by plasmid gap repair using the gene fragment with flanking homology to the linearized plasmid vector. Positive colonies were purified through serial passage on ura$^-$ media. The resulting colonies were sequenced to confirm correct integration. Similarly, plasmid pRS425 was used to insert genes CNAG_02086, and CNAG_02087. These plasmids do not contain a Gal1 promoter. Therefore, the Gal1p was amplified from plasmid pYES2/CT. Primers were designed to amplify Gal1p with overlap of part of plasmid pRS425, gene CNAG-02086 ATG forward primer, CNAG_02086 with TAA and overlap of pRS425, as well as CNAG-02087 ATG forward primer, CNAG_02087 with TAA and overlap of pRS425. These fragments were then co-transformed along with the linearized vector into *Sc* BY4741. Transformants were selected on synthetic leu$^-$ dropout media. Two additional strains were constructed by co-transforming pYES2/CT+Cer1 along with pRS425+Cer2 or pRS425+Cer3. These transformants were passaged on synthetic leu$^-$ura$^-$ media to obtain pure isolates.

Protein microsomal preparation

Microsomal isolation method was adapted from (Ternes, Wobbe et al. 2011) with modifications. Briefly, cells of *S. cerevisiae* strain BY4741 expressing gene of interest (Cer1, Cer2, Cer3, Cer1+Cer2, or Cer1+Cer3) was grown in 10 ml YNB (containing the appropriate amino acid dropout mix) + 2 %glucose, overnight at 30°C. The next day, these cells were washed twice with PBS and transferred to 300 ml YNB+1% galactose+1% raffinose media and allowed to grow overnight. These cells were then centrifuged and the pellet was resuspended in 1-2 ml lysis buffer (20mM HEPES/KOH pH 7.4, 25mM KCl, 2mM $MgCl_2$, 250mM sorbitol) and 50µl protease inhibitor cocktail (Thermo scientific, Waltham, MA). ~1ml volume of glass beads was added to 1ml lysate in a tube and this slurry was vortexed vigorously for ~2 hours. Cell debris were removed by centrifugation at 1000×g, 4°C, for 3 mins. Supernatant was loaded on to a 60% sucrose cushion (w/w), and spun in an ultracentrifuge at 4°C, 24,000 RPM, for 1 hour. The microsomes were isolated from the interphase with a Pasteur pipette and stored at -80°C.

Fluorescent cryptococcal ceramide synthase assay

An assay for ceramide synthase activity was adapted from (Kim, Qiao et al. 2012, Tidhar, Sims et al. 2015) with minor changes. Microsomes of overexpressed ceramide synthase were used as enzymes for these reactions. Briefly, NBD- Sphingosine or NBD-Phytosphingosine (Avanti Polar lipids, Alabaster, AL) was combined with Fatty Acyl CoA of varying chain lengths (C18, C24, C26) (Avanti Polar lipids, Alabaster, AL) as a substrate mixture. A 100µl reaction was carried out using reaction buffer (20 mM Hepes, pH 7.4, 25 mM KCl, 2 mM $MgCl_2$, 0.5 mM DTT,

0.1% (w/v) fatty acid-free BSA) along with 10μM NBD sphingosine and 50μM fatty acyl CoA. 150μg of microsomal protein was added per reaction, as measured in a Bradford assay (effective protein amount empirically determined). The reactions were then incubated at 35°C for 90 minutes. The reactions were then stopped with 2:1 chloroform:methanol, followed by gentle vortexing. The lipids were then extracted and dried in a speed vacuum (SPD 2010) followed by resuspension in 100% methanol. The reaction was analyzed by thin layer chromatography, using chloroform/methanol/water (8:1:0.1, v/v/v) as the solvent mixture.

Virulence studies and histology analysis in a murine mouse model of cryptococcosis

3-4 weeks old female CBA/JCrHsd (Harlan Laboratories, Indianapolis, IN, USA) mice were used for all experiments. Mice were anesthetized with 60 μl xylazine/ketamine mixture containing 95 mg ketamine and 5 mg xylazine per kilogram of body weight prior to infection. *Cn* strains WT H99, *Δcer1, Δcer2, Δcer3 and Δcer1+CER1* were grown overnight in YPD broth at 30°C. The next day, cells were pelleted, washed twice and resuspended in PBS at a concentration of 3.5×10^7 cells/ ml. For survival studies, ten CBA/JCrHsd mice per strain were infected with 7×10^5 cells for each strain in a volume of 20 μl through nasal inhalation. For tissue burden analysis, 9 mice per strain were used. Lung, brain, kidney, liver and spleen were excised and homogenized in 10ml PBS using stomacher 80 (Seward, UK) for 2 min at high speed. Serial dilutions were plated in duplicate on YPD agar plates and incubated for 48-72 hours at 30°C for assessment of CFU per organ. For histopathology analysis, 3 mice per experimental group were used. Mice organs were fixed in 3.7% formaldehyde in paraffin and stained with haematoxylin and eosin and mucicarmine. Staining was performed in part by McClain Labs (Smithtown, NY), as well as by Research Histology Core at Stony Brook University.

Extraction and mass spectrometry analysis of yeast sphingolipids

For extraction of lipids, cells of wildtype, mutant and reconstituted strains were grown overnight in YPD at 30°C. The next day these cells were washed and transferred to DMEM (pH 4.0 or 7.4) and grown in shaking condition at 37°C + 5% CO_2 for about 16 hours. These cells were washed and counted for lipid extraction. Briefly, 10^8 cells for each replicate were pelleted in a glass tube in which mandala extraction buffer was added and extraction was performed as described in (Mandala, Thornton et al. 1995). Further extraction was performed according to the methods of Bligh and Dyer (Bligh and Dyer 1959). After measuring the dry weights, the samples were subject to base hydrolysis (Clarke and Dawson 1981). The extracts were dried in a centrifuge under a vacuum (SPD 2010, ThermoFisher Scientific, Waltham, MA). All internal standards were added prior to lipid extraction. The following

internal standards from Avanti Polar Lipids (Alabaster, AL) were used: Sphingosine (d17:1), D-erythro-sphingosine (C17 base), N-08:0 Phytosphingosine (N-octanoyl-4-hydroxysphinganine)(Saccharomyces Cerevisiae), sphinganine (d17:0) D-erythro-sphinganine (C17 base), Sphingosine-1-Phosphate (d17:1) D-erythro-sphingosine-1-phosphate (C17 base) and C17 Ceramide (d18:1/17:0) N-heptadecanoyl-D-erythro-sphingosine.

For the mass spectrometry analysis, the dried extracts were separated on a Thermo Accela HPLC system (San Jose, CA) after dissolving in 150 µL of ammonium formate (1mM) with 0.2% formic acid in methanol. We used a Peeke Scientific Spectra C8 (Redwood City, CA) HPLC column (150 x 3 mm) into which 10 µl samples were injected. The buffers used for the runs were as follows: Buffer A (2mM ammonium formate and 0.2% formic acid(FA)) and buffer B, ammonium formate (1mM) with 0.2% FA in methanol. A gradient using buffer A and B was used, starting with 70% B with an increase to 90% over 5 minutes, followed by a ramp to 99% B over 9 minutes. The column was equilibrated with initial conditions for 8 minutes at a flow rate of 500 µL/min. The HPLC was coupled to the HESI source of a Thermo TSQ Quantum Ultra triple quadrupole mass spectrometer (San Jose, CA). The sphingolipid profile was performed using positive ion mode. With the high voltage set to 3.5 kV, vaporizer temperature at 400ºC, sheath gas pressure at 60, auxiliary gas pressure at 15 and a capillary temperature of 300ºC. The collision cell was operated at 1.5 mTorr of argon. For the duration of the run, transitions for each lipid species were monitored at 100 ms or 50 ms dwell time. 20 lipid standards for our profile from Avanti (Alabaster, AL) were used to develop calibration curves and these curves were then used for lipids species to be monitored. Processing of the samples was done using Thermo Xcalibur 2.2 Quan Browser software and exported to excel for reporting results.

***In vitro* growth studies**

From overnight YPD broth cultures of *Cn* WT, *Δcer1* and *Δcer1+CER1* were washed twice in phosphate buffered saline (PBS), resuspended and diluted into 10ml DMEM (buffered with HEPES, pH 4.0 or pH 7.4) to a final density of 10^4 cells/ml and incubated in shaker incubator at 37°C with 5% CO_2. Aliquots were taken at time points indicated and serial dilutions were plated on YPD agar for assessment of CFU. For cell wall stability, cells were spotted in serial dilutions on YPD plates with 0.05% SDS. For osmotic stress, cells were spotted on YPD containing 2mM H_2O_2.

Transmission Electron microscopy

Cn strains were grown overnight in YPD at 30°C with shaking. The next day, these cells were washed, counted and transferred to DMEM (pH 4.0 or 7.4) and grown in shaking condition at 37°C +5% CO_2 to mimic physiological

conditions. After 24 hours of growth, these cells were washed with phosphate buffered saline, and fixed in 3% EM grade glutaraldehyde solution for 2 hours. For supplementation experiments, cells grown in physiological condition as mentioned earlier were supplemented with 50µM ceramides mix (Matreya LLC, PA). For sample preparation, after glutaraldehyde fixation, cells were rinsed in 0.1M phosphate buffer pH7.4 and dispersed and embedded in ultra-low gelling temperature agarose. Tubes containing these cells were then cooled and agarose samples were chopped into cubes of smaller size. Post fixation of these samples was done by rinsing with aqueous potassium permanganate, and then further rinsed and treated with sodium meta periodate. This was followed by another rinse, and ultimately dehydrated through a graded ethanol series. After dehydration samples were embedded in Spurr's resin and polymerized in a 60°C oven. For sectioning, ultrathin sections of 80nm were cut with a Leica EM UC7 ultramicrotome and placed on 300 mesh copper grids. Sections were then counterstained with uranyl acetate and lead citrate and viewed with a FEI TeCnai12 BioTwinG^2 transmission electron microscope. Digital images were acquired with an AMT XR-60 CCD Digital Camera system.

Replicative lifespan studies

Replicative lifespan for WT and mutant *Cn* strains was measured by microdissection according to (Park, McVey et al. 2002, Bouklas, Jain et al. 2017) with minor adjustments. Briefly, Cells of *Cn* were plated and incubated at 37°C. The bud of these cells were followed by identifying the first bud and following its increase in size during the cell cycle. The daughter cells were separated from mother cell at the end of each division (1-2 hours) with the help of a 50 µm fiber optic needle (Cora Styles) on a tetrad dissection Axioscope A1 microscope (Zeiss) at 100x magnification. Replicative lifespan of each cell was determined as sum of the total buds until the mother cells fail to divide any further.

Glucose dependent medium acidification to measure plasma membrane H^+-ATPase

Glucose-dependent medium acidification was monitored by a modification of a procedure described previously (Perlin, Brown et al. 1988, Soteropoulos, Vaz et al. 2000). Cultures of *Cn* strain WT, Δ*cer1*, Δ*cer1+CER1,* Δ*gcs1* were grown to mid-log

Phase in YPD. The next day, these cells were transferred to DMEM at pH 4.0 and allowed to grow under shaking conditions for 24 hours. These cells were then harvested and washed using 100mM KCl, pH 5.0. These pellets were then resuspended in 10ml KCl, pH 5.0 and incubated under shaking condition at 30 ℃. These samples were then stored at 4 ℃ overnight prior to use. For the assay, cells were concentrated to a final A590 of approximately 2.0. 20

µl cells along with 155 µl of bromophenolblue (50 µg/ml) in 100mM KCl, pH 5.0. 20 µl 20% (w/v) glucose was added to initiate the reaction. Medium acidification was monitored at 590 nm over a period of 5 hours (data point every 3 mins) in a microplate reader (SpectraMax M5).